Research article

Developing diagnostic biomarkers for Alzheimer's disease based on histone lactylation-related gene

Shaobo Guo [a,b,c], Wenhui Zhu [a,b,c], Yuting Bian [a,c], Zhikai Li [a,c], Heng Zheng [a,c,d]
, Wenlong Li [a,c,e], Yi Yang [a,c], Xuzheng Ji [a,c], Biao Zhang [a,c,*]

[a] The Affiliated Hospital of Nanjing University of Chinese Medicine, Department of Geriatric, Nanjing, China
[b] Key Laboratory for Metabolic Diseases in Chinese Medicine, First College of Clinical Medicine, Nanjing University of Chinese Medicine, Nanjing, China
[c] Jiangsu Provincial Hospital of Traditional Chinese Medicine, Nanjing, China
[d] Zhenjiang Hospital of Chinese Traditional And Western Medicine, Zhenjiang, China
[e] Liyang Hospital of Chinese Medicine, Liyang, China

ARTICLE INFO

ABSTRACT

Background: Research underscores the significant influence of histone lactylation pathways in the progression of Alzheimer's disease (AD), though the molecular mechanisms associated with histone lactylation-related genes (HLRGs) in AD are still insufficiently investigated.
Methods: This study employed datasets GSE85426 and GSE97760 to identify candidate genes by intersecting weighted gene co-expression network analysis (WGCNA) module genes with AD-control differentially expressed genes (DEGs). Subsequently, machine learning refined key genes, validated by receiver operating characteristic (ROC) curve performance. Gene-set enrichment analysis (GSEA) explored the molecular mechanisms of these diagnostic markers. Concurrently, the association between the diagnostic genes and both differential immune cells and immune responses was examined. Furthermore, a ceRNA and gene-drug network was developed. Finally, the expression of the selected genes was validated using brain tissues from AD model mice.
Results: This study identified five genes (ARID5B, NSMCE4A, SESN1, THADA, and XPA) with significant diagnostic utility, primarily enriched in olfactory transduction and N-glycan biosynthesis pathways. Correlation analysis demonstrated a strong positive association between all diagnostic genes and naive B cells. The ceRNA regulatory network comprised 7 miRNAs, 2 mRNAs, and 25 lncRNAs. Additionally, 33 drugs targeting the diagnostic genes were predicted. Following expression validation through training and validation sets, three genes (ARID5B, SESN1, XPA) were ultimately confirmed as biomarkers for this study. RT-qPCR and Western blot analyses revealed upregulated expression of ARID5B, SESN1, and XPA in the cerebral tissue of AD model mice.
Conclusion: Three histone lactylation-linked genes (ARID5B, SESN1, XPA) were identified as potential AD biomarkers, indicating a strong association with disease progression.

* Corresponding author. The Affiliated Hospital of Nanjing University of Chinese Medicine, Department of Geriatric, Nanjing, China.
E-mail addresses: 1227403718@qq.com (S. Guo), 1356335464@qq.com (W. Zhu), 707101828@qq.com (Y. Bian), 1760726337@qq.com (Z. Li), 2557811897@qq.com (H. Zheng), 1127813186@qq.com (W. Li), 1169501788@qq.com (Y. Yang), 1341020356@qq.com (X. Ji), zhangbiao1969@163.com (B. Zhang).

1. Introduction

Alzheimer's disease (AD) is a progressive neurodegenerative disorder marked by amyloid-beta (Aβ) plaques and tau neurofibrillary tangles [1]. AD leads to a decline in cognitive and functional abilities, significantly disrupting daily activities. Clinical symptoms include memory loss, language difficulties, behavioral changes, and impaired decision-making. The global prevalence of AD is increasing, with the 2021 International AD Report estimating around 55 million patients worldwide, projected to reach 152 million by 2050 [2]. Two-thirds of this population resides in low- and middle-income countries [3]. AD primarily affects individuals over sixty-five, with incidence rising with age and a higher prevalence in females. The United States Food and Drug Administration has approved five pharmacological treatments for AD: donepezil, rivastigmine, galantamine, memantine, and a memantine-donepezil combination [4]. Current treatments are limited, costly, and do not address the root cause, only alleviating symptoms and slowing progression. Thus, discovering novel biomarkers for detection, diagnosis, and therapeutic targeting is critically important.

Recent insights underscore the pivotal role of epigenetic modulation in AD, particularly emphasizing histone modification as a crucial component of the epigenetic landscape [5]. Histone lactylation, a novel epigenetic modification, emerges from the Warburg effect, leading to histone lysine lactylation, which in turn influences chromatin gene transcription and gene expression regulation. Histone post-translational modifications (HPTMs) are key epigenetic mechanisms orchestrating a wide array of biological functions [6]. IThe accumulation of lactate is closely tied to neural activity. In the AD mouse model (APP/PS1), lactate content in the frontal cortex increases with age, surpassing levels observed in control mice [7]. In the early stages of AD, such as mild cognitive impairment (MCI), lactate levels in the posterior cingulate cortex negatively correlate with memory performance [8]. Patients with AD exhibit significantly elevated lactate concentrations in their cerebrospinal fluid compared to age-matched healthy individuals [9]. According to reports, in Alzheimer's Disease (AD), histone lactylation has been observed in microglia, the primary immune cells of the central nervous system. Specifically, lactylation at the H4K12 site (H4K12la) increases with the appearance of amyloid-β (Aβ) plaques. This lactylation at H4K12 enhances the transcription of glycolytic genes, thereby promoting glycolytic activity and forming a positive feedback loop. This exacerbates microglial dysfunction and neuroinflammation [10].

Histone deacetylases (HDACs) can regulate the lactylation levels of histone lysine and play a crucial role in AD. There are 18 HDAC subtypes, divided into four classes (Class I, II, III, and IV). HDAC1-3, in particular, is pivotal in AD. HDAC1 possesses neuroprotective effects and can stimulate DNA repair, preventing brain aging and functional decline in neurodegenerative diseases [11]. The interaction between HDAC1 and SIRT1 orchestrates a neuroprotective response by mitigating DNA damage [12]. Although HDAC2 is highly similar to HDAC1, it exhibits neurotoxicity. Overexpression of HDAC2 in mouse models has been linked to a decline in synapse density and plasticity, impeding memory consolidation [13]. Knockdown of HDAC2 in AD mice using shRNA significantly improves hippocampal-dependent memory performance and synaptic plasticity [14]. DAC3, the deacetylase with the most significant effect on histone lactylation, has a complex role in AD [15]. Most current research suggests that inhibiting Class I HDAC improves cognitive impairment in AD, although the majority of these studies concentrate on Class I HDAC proteins as a whole rather than on specific HDAC subtypes [16,17]. Not all HDACs have adverse effects on AD, making further research on other modifications of HDAC1-3 subtypes valuable and promising.

This study utilized the GSE85426 dataset related to AD from the GEO database as the training set, while the GSE97760 dataset served as the validation set. Through differential gene expression analysis and various bioinformatics methods such as WGCNA, three histone lactylation-related diagnostic genes were identified. The diagnostic value of these genes was subsequently evaluated. Their gene and protein expression levels were validated using the APP/PS1 mouse model. Additionally, pathways and biological processes enriched by the diagnostic genes were explored, gene expression data for immune cell infiltration was analyzed, and a ceRNA network along with a gene-drug network was constructed. This research provides a theoretical basis for discussing the molecular mechanisms of AD based on histone lactylation-related genes (HLRGs).

2. Materials and methods

2.1. Source of data

The GSE85426 and GSE97760 datasets were sourced from the GEO database. The GSE85426 dataset, comprising RNA-seq data of peripheral blood cells from 90 AD samples and 90 control samples, was used as the training cohort. The GSE97760 dataset, including RNA-seq data of whole blood from 9 AD samples and 10 control samples, served as the validation cohort. From previous reports, three HLRGs, namely HDAC1, HDAC2, and HDAC3, were identified [15,18].

2.2. Identification of differentially expressed genes (DEGs)

First, DEGs between the AD and control groups were identified using the limma package (v 3.50.1) [19] in the training cohort, with an adjusted P value < 0.05 and $|\log_2 FC| > 0.5$. The results of the differential analysis were illustrated using a volcano plot generated by the ggplot2 package (v 3.3.5) [20]. Additionally, the expression levels of the top 10 up- and down-regulated genes were visualized using box plots.

2.3. Filtering for key module genes by weighted gene co-expression network analysis (WGCNA)

In the GSE85426 dataset, the ssGSEA scores of the samples were computed using the GSVA package (v 1.42.0) [21] based on the HLRGs. The co-expression network was constructed using WGCNA (v 1.70–3) [22]. Initially, samples underwent clustering, and outliers were pruned to enhance the robustness of the analytical framework. A soft threshold (β) was then calibrated to approximate a scale-free network architecture. The resulting cluster dendrogram was generated through the computation of adjacency and similarity measures. Modules were delineated using a dynamic tree-cutting algorithm. Next, a correlation analysis between module eigengenes and ssGSEA scores was conducted, identifying the module with the highest correlation coefficient as the primary focus. Finally, genes within the key module with |Gene Significance (GS)| > 0.5 and |Module Membership (MM)| > 0.8 were identified as key module genes for subsequent analysis.

2.4. Screening and enrichment analysis of candidate genes

Candidate genes were filtered by overlapping key module genes and DEGs. Using the clusterProfiler package, targeted enrichment analysis within Gene Ontology (GO) and the Kyoto Encyclopedia of Genes and Genomes (KEGG) was conducted to decode the biological functions and pathways associated with the selected candidate genes [23]. Significant enrichment was defined by an adjusted P value < 0.05. Finally, a protein-protein interaction (PPI) network, based on candidate genes, was constructed using the STRING database's analytical resources.

2.5. Machine learning screening and performance evaluation of key genes

Least absolute shrinkage and selection operator (LASSO) regression profiling was conducted using the glmnet package (v 4.1–4) [24] to identify key genes. Subsequently, a logistic regression model was crafted using the glm function, centered on pivotal genes, to forecast the risk for AD. The discriminatory capacity of the diagnostic model between control and AD cohorts was evaluated by plotting receiver operating characteristic (ROC) curves for the model within the GSE85426 and GSE97760 datasets. The area under the curve (AUC) values of the ROC curves were computed using the pROC package (v 1.18.0) [25].

2.6. Identification of diagnostic genes

To determine the diagnostic value of key genes in AD, ROC curves for each key gene were plotted using the GSE85426 and GSE97760 datasets. Genes with AUC values ≥ 0.7 in both datasets were selected as diagnostic genes for this study. To further explore the association between prognostic genes and HLRGs, Spearman correlation analysis was conducted using the GSE85426 dataset, with significance defined as P < 0.05. To further characterize the expression of diagnostic genes in different anatomical regions of the brain, the expression of diagnostic genes in different anatomical regions of the brain of AD and control samples was analyzed based on the AlzData database (http://www.alzdata.org/).

2.7. Gene set enrichment analysis (GSEA)

Within the GSE85426 dataset, samples were stratified into groups based on high and low expression profiles of the diagnostic genes. GSEA was then performed using the KEGG geneset as the background to identify enriched regulatory pathways and biological functions between the high- and low-expression groups. The top five KEGG pathways showing significant enrichment were subsequently visualized.

2.8. Immuno-infiltration analysis

To further explore the relationship between immune infiltration and diagnostic genes, the proportions of 22 immune cell subtypes for each sample were computed using the CIBERSORT algorithm [26] in the training cohort. Differential immune cell populations between AD and control groups were then compared, and the results were visualized with box plots. Additionally, correlation analysis was performed between differential immune cells and diagnostic genes.

2.9. Construction of the competing endogenous RNA (ceRNA) network

ceRNA is an action element that can compete for binding to RNAs. miRNAs are at the center of regulation in lncRNA-miRNA-diagnostic gene analysis, and when miRNAs are competed for binding by lncRNAs, the level of transcription of diagnostic genes regulated by miRNAs rises. To further investigate the molecular regulatory mechanism of diagnostic genes, we utilized the miRDB, miRWalk, and ENCORI databases to predict the upstream miRNAs of the diagnostic genes. We then identified the key miRNAs by taking the intersection of the three predictions. Subsequently, we used the miRcode and ENCORI databases to predict the upstream lncRNAs of these miRNAs. After predicting the upstream lncRNAs using both databases, we identified the key lncRNAs by taking the intersection of the predictions from miRcode and ENCORI. Finally, we visualized the lncRNA-miRNA-diagnostic gene regulatory network using Cytoscape software [27].

2.10. Construction of diagnostic gene-drug interaction network

To explore new therapeutic targets for AD treatment, small-molecule drugs targeting diagnostic genes were predicted. Initially, drugs targeting the diagnostic genes were identified using the CTD database (http://ctdbase.org/) with a reference count greater than 1. Based on this predictive analysis, a gene-drug network was constructed for diagnostic application.

In the training set (GSE85426) and the validation set (GSE97760), the box-and-line plots of the expression levels of the diagnostic genes were plotting, comparing AD with the control group, respectively. Then, a comprehensive analysis was conducted based on these expression levels.

2.11. Animals

Ten SPF-grade 8-month-old APPswe/PSEN1dE9 mice and ten SPF-grade 8-month-old wild-type (WT) littermates were obtained from Changzhou Cavins Laboratory Animals Co., Ltd. (Changzhou, China; license number: SCXK (Su) 2021-0013). APP/PS1 (APPswe/PSEN1dE9) mice served as the AD model, while WT littermates constituted the control group. Mice were maintained under a 12-h light-dark cycle in a controlled environment, with ad libitum access to food and water, and a stable ambient temperature of 22–25 °C.

2.12. Material collection

Prior to sample collection, the mice underwent a 12-h fasting period with unrestricted access to water. They were then intraperitoneally injected with 20 mg/kg of pentobarbital sodium. Once anesthetized, brain tissue was extracted. Brains from a randomly selected trio of mice in each cohort were fixed in 4 % paraformaldehyde, while the remaining samples were immediately placed in cryotubes, snap-frozen in liquid nitrogen, and stored at −80 °C for subsequent qPCR and Western blot analyses.

2.13. Immunohistochemistry

Paraffin sections were deparaffinized to water, followed by antigen retrieval. The sections were then incubated in a 3 % hydrogen peroxide solution at room temperature for 20 min to inhibit endogenous peroxidase activity. Serum blocking was performed at room temperature for 30 min. After removing the blocking solution, the sections were treated with the diluted primary antibody and incubated overnight at 4 °C. The primary antibodies used were Aβ (1:200, Boster Biological Technology, Wuhan, China) and C-caspase3 (1:200, Affinity Biosciences, Tianjin, China). Following a PBS wash, the slides were incubated with the appropriate HRP-labeled secondary antibody at room temperature for 50 min. DAB was then applied for color development, and hematoxylin was used for nuclear counterstaining. High-quality images were captured in several fields of view for each sample.

2.14. Western blotting

Approximately 50 mg of mouse brain tissue per group was collected and ground on ice, then total protein was extracted by adding PIPA strong lysis solution (Beyotime Biotechnology, Shanghai, China) and protease phosphatase inhibitor (NCM Biotech, Suzhou, China). Protein levels were measured using a BCA protein assay kit (NCM Biotech, Suzhou, China). The extracted proteins were separated by SDS-PAGE electrophoresis and then transferred onto a PVDF membrane through a methodical membrane transfer technique. The membrane was blocked in a 5 % non-fat milk solution to prevent non-specific binding for 70 min. After blocking, the membrane was incubated overnight at 4 °C with primary antibodies specific to ARID5B, XPA, and SESN1. The process concluded with a 2-h incubation with the corresponding secondary antibody.

Band visualization was achieved through enhanced chemiluminescence (ECL), and densitometry of protein bands was conducted using tubulin and GAPDH as internal standards. Quantitative assessment was performed with ImageJ, and statistical analysis was conducted using GraphPad Prism 9.5. Details of the antibodies used are listed in Table 1.

2.15. Quantitative Real-time PCR

Approximately 50 mg of mouse brain tissue was collected and ground on ice, followed by the addition of Trizol to extract total RNA,

Table 1
The antibody information used in the Western Blotting analysis.

ANTIBODY	COMPANY	CATALOG NO.	MOLECULAR WEIGHT (kDa)
GAPDH	Signalway Antibody	#52902	36
ARID5B	GeneTex	GTX131249	132
XPA	proteintech	16462-1-AP	40–50
β Tubulin	proteintech	10094-1-AP	50–55
SESN1	affinity	DF4494	57
β Amyloid	Boster	PB9091	
Caspase3	affinity	AF7022	
Goat Anti-Rabbit igG (H + L)	proteintech	SA00001-2	

which was evaluated using a spectrophotometer. RNA from each group was then reverse transcribed using HiScript II Q RT SuperMix for qPCR (Vazyme, Nanjing, China). Primers were synthesized by Shanghai Sangon Biotech Company based on the gene sequences in GenBank. According to the manufacturer's instructions, qPCR was performed on an Applied Biosystems PCR 7500 using ChamQ SYBR qPCR Master Mix (Vazyme, Nanjing, China). Gene mRNA levels were quantified relative to GAPDH and calculated using the $2^{-\Delta\Delta}$CT method, with primer sequences detailed in Table 2.

2.16. Statistical analysis

All bioinformatics analyses were conducted using the R language. Spearman correlation analysis was performed to evaluate correlations, and the Wilcoxon test was used to identify differences across groups.

3. Results

3.1. Acquisition of DEGs and key module genes

Of the 975 DEGs were identified between the AD and control groups, with 586 were up-regulated and 389 were down-regulated (Fig. 1A, Additional file 1). The expression levels of the top 10 most significantly modulated genes were illustrated in a box plot, with up-regulated genes on the left and down-regulated genes on the right (Fig. 1B). To explore gene associations with ssGSEA-derived scores, WGCNA was utilized. Clustering of samples revealed a single outlier, which was removed, and the remaining samples were re-clustered. Subsequent to outlier removal, the samples underwent a secondary clustering process (Additional file 2A, 2B). Setting a soft threshold of 20, with R^2 = 0.85 (red line) and average connectivity near 0, the gene interaction network aligned with a scale-free distribution (Fig. 1C). Thirteen modules were identified using the dynamic tree-cutting algorithm (Fig. 1D). Among these, the MEturquoise module exhibited the highest correlation with ssGSEA scores (Cor = 0.8, P = 2e-41) (Fig. 1E), making it pivotal. Consequently, 1174 genes within this module were designated as key module genes for further analysis (Fig. 1F). Overall, these results provided valuable insights into the gene expression changes associated with AD and highlight the importance of the MEturquoise module in relation to disease pathology.

3.2. Identification and functional annotation of candidate genes

A total of 382 candidate genes, including SESN1, THADA, MRPS23, NSMCE4A, ATP9B, GGA1, KEAP1, THYN1, TAF11, and IDH3B, were identified by overlapping 1174 key module genes with 975 DEGs (Fig. 2A). Enrichment analyses associated these candidate genes with 85 GO annotations and 7 KEGG pathways. The genes were primarily enriched in GO categories such as histone acetylation and histone modification (Fig. 2B, Additional file 3), while KEGG enrichment results included pathways like basal transcription factors and the cell cycle (Fig. 2C, Additional file 4). The PPI network comprised 332 nodes and 1132 edges (Fig. 2D), including 12 down-regulated genes and 320 up-regulated genes.

3.3. Identification and expression of key genes

LASSO is a regularization method for linear regression. Unlike traditional regression methods, LASSO is able to select the variables with the strongest predictive power in the case of high-dimensional data, thus improving the explanatory and predictive performance of the model. A total of 13 key genes (SESN1, THADA, MRPS23, NSMCE4A, ATP9B, GGA1, TFG, ARID5B, XPA, CCND2, LYAR, BTF3P11, and SLBP) were identified using LASSO regression analysis (Fig. 3A and B). The ROC curves for the GSE85426 and GSE97760 datasets indicated that the diagnostic model performed well, with AUC values greater than 0.7 (Fig. 3C and D).

3.4. Screening and GSEA analysis of diagnostic genes

In this study, we identified five diagnostic genes (ARID5B, NSMCE4A, SESN1, THADA, and XPA) by comparing the AUC values of key genes in the GSE85426 and GSE97760 datasets (Fig. 4A and B). Furthermore, we found that diagnostic genes were highly correlated with HLRGs, and in frontal cortex brain tissue, SESN1 expression was significantly higher in AD than control (Additional file 5). Further analysis using GSEA revealed interesting findings. ARID5B was not enriched in any KEGG signaling pathway, SESN1 was enriched in one pathway, NSMCE4A and XPA were enriched in two pathways each, and THADA was enriched in 14 pathways. Notably, NSMCE4A, SESN1, THADA, and XPA were predominantly enriched in KEGG terms associated with low-expression groups such as

Table 2
The Primer sequences used in the Quantitative Real-Time PCR.

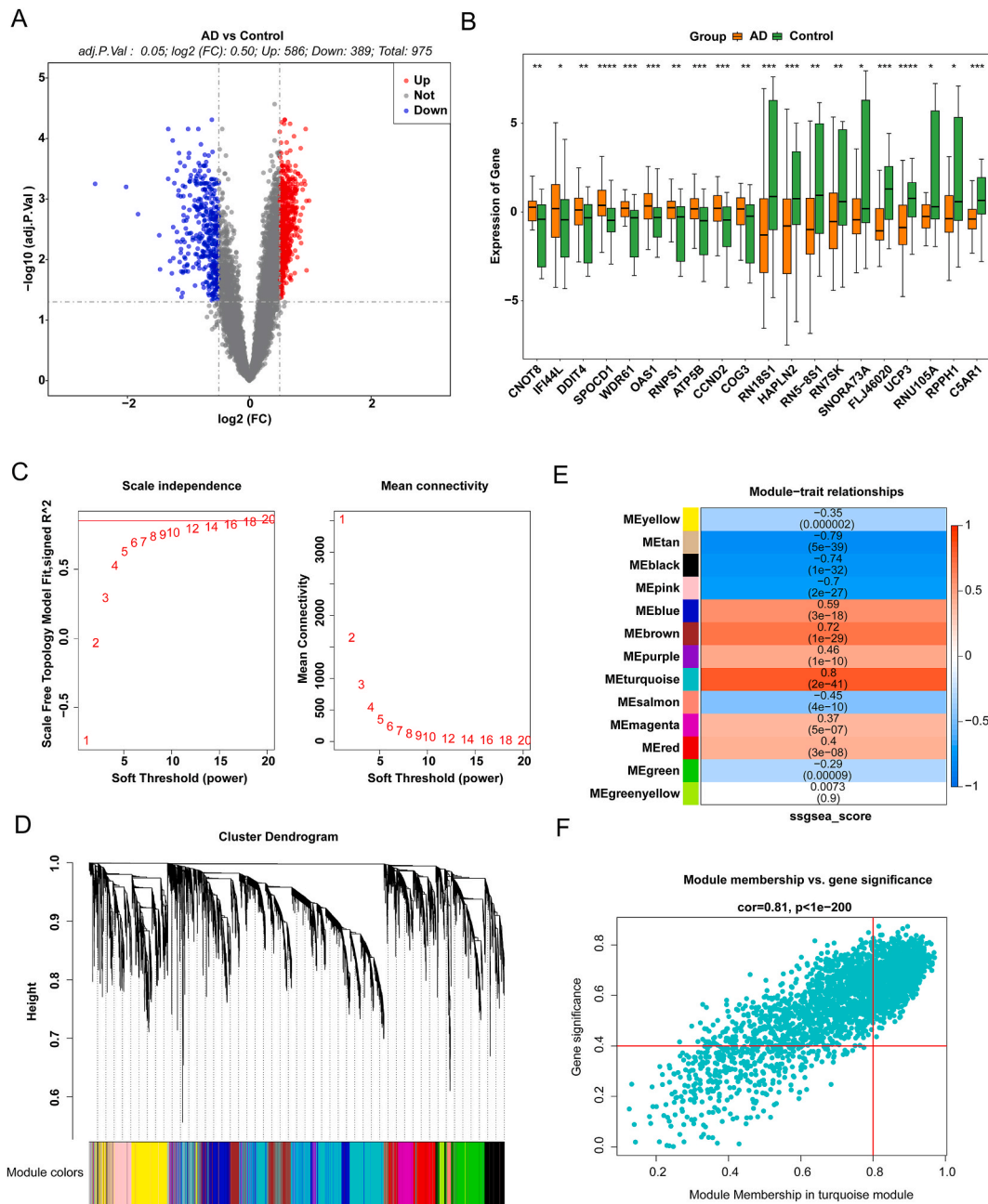| mRNA	Forward Primer (5′- 3′)	Reverse Primer (5′- 3′)
ARID5B	ACAACGAACAGTCCTCCAAGTATGC	CTGCCGCTGCCACCTTCTTATC
SESN1	CCAAGCAGGTTCATCCCAGAGAAG	AGACGACCCAAAGCAGCAAAGG
XPA	ACCAAGACAGAAGCGAAGCAAGAG	ACTGTGAATGGCGTGGGTTCTTC
GAPDH	AGGTCGGTGTGAACGGATTTG	TGTAGACCATGTAGTTGAGGTCA

Fig. 1. Selection of differentially expressed genes (DEGs) and key module genes in alzheimer's disease (AD). (**A**) Volcano plot and (**B**) box plot for DEGs between AD and Control groups. (**C**) A soft-threshold analysis set with R^2 = 0.85 and a soft-threshold value β of 20. (**D**) Clustering dendrogram of all genes based similar expression patterns. Each branch represents a gene, and each color at the bottom represents a co-expression module. (**E**) Heatmap of the correlation between modules and ssGSEA scores based on three histone lactylation-related genes (HLRGs), where red indicates positive correlation and blue indicates negative correlation. (**F**) A scatterplot of gene significance (GS) for weight vs. module membership (MM) in the turquoise module. (For interpretation of the references to color in this figure legend, the reader is referred to the Web version of this article.)

olfactory transduction (Fig. 5A–D). The NSMCE4A high-expression group was enriched to other glycan degradation, while the XPA high-expression group was enriched to lysosome (Fig. 5A and D). Moreover, the THADA high-expression group demonstrated enrichment in N-glycan biosynthesis, other glycan degradation pathways, among others (Fig. 5C, Additional file 6). Overall, these findings shed light on the diagnostic and prognostic potential of the identified genes and their relevance to specific signaling pathways and gene expression levels.
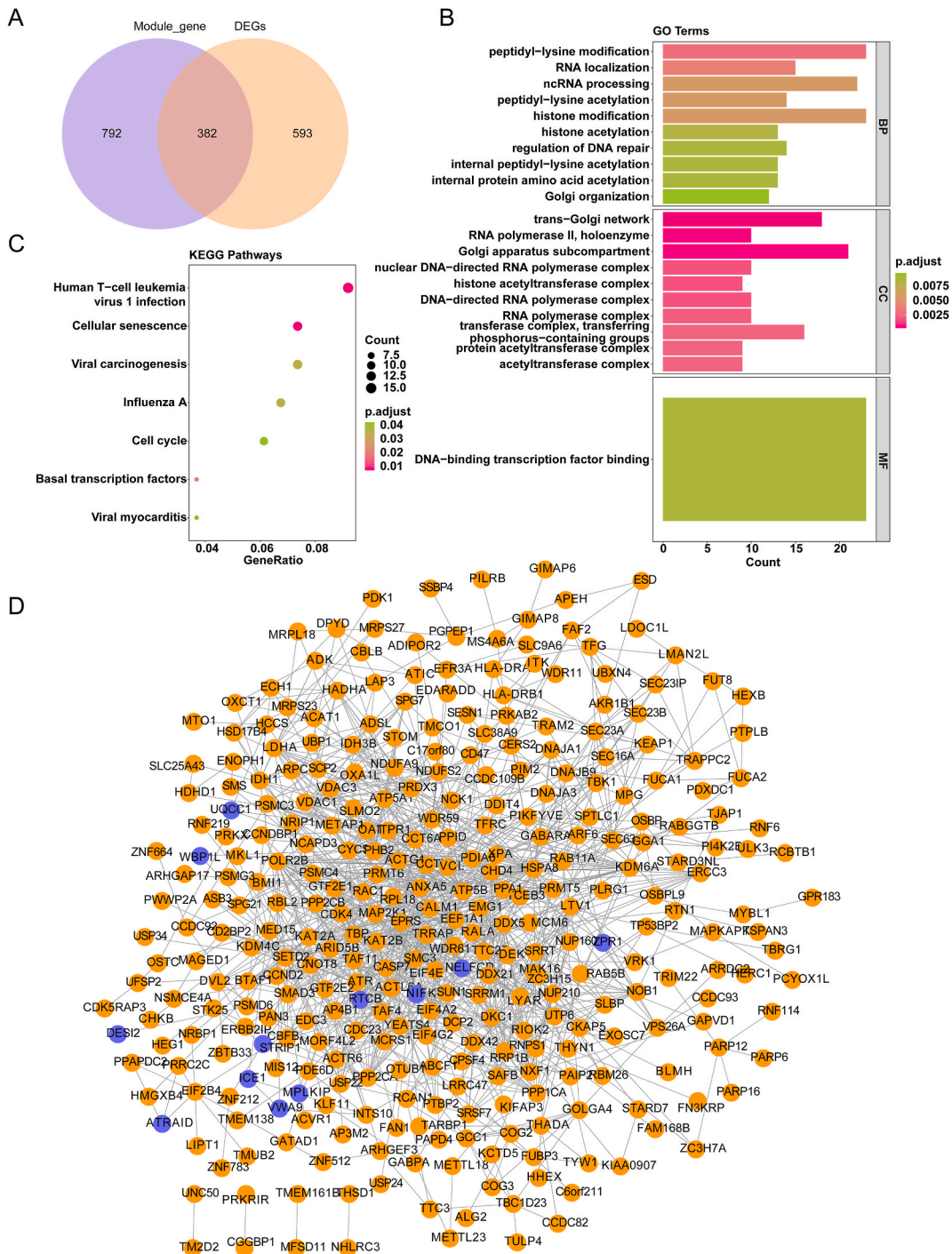
Fig. 2. Functional enrichment analysis and Protein-protein interactions (PPI) network of candidate genes. (**A**) Venn diagram of the intersected genes between DEGs and core genes of the module. (**B**) Bar chart for the Gene Ontology (GO) enrichment of candidate genes, selecting and plotting the top 10 most significant functions from each section. (**C**) Bubble chart for Kyoto Encyclopedia of Genes and Genomes (KEGG) enrichment of the candidate genes. (**D**) The PPI network after analyzing the 382 candidate genes, where the blue circles represent down-regulated genes, and the red circles represent up-regulated genes. (For interpretation of the references to color in this figure legend, the reader is referred to the Web version of this article.)
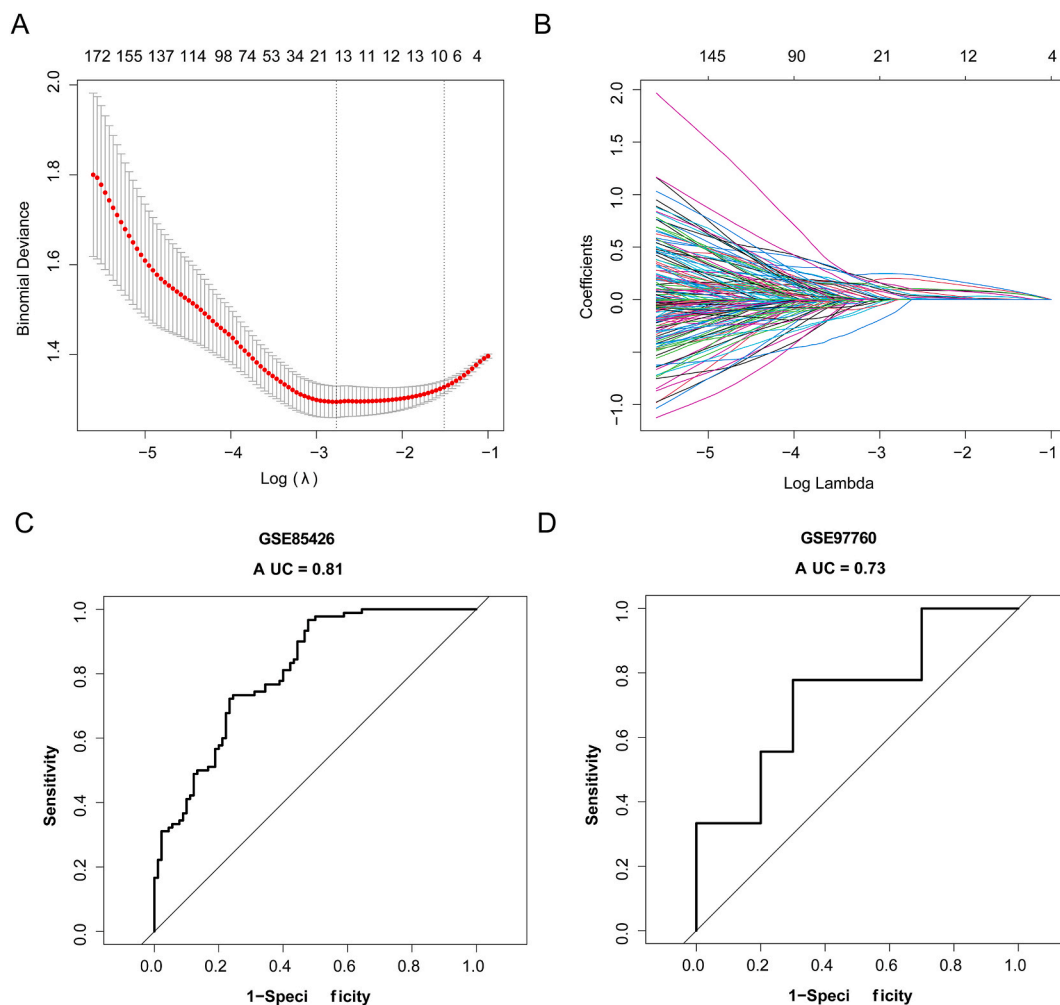
Fig. 3. Machine learning screening and model evaluation. (**A**) Least absolute shrinkage and selection operator (LASSO) regression analysis of candidate genes, with ten-fold cross-validation for parameter adjustment. (**B**) Lasso coefficient spectrum chart, where the x-axis represents the logarithm of lambdas, and the y-axis represents the coefficient of variables. As lambdas increase, the variable coefficients tend towards 0. When reaching the optimal lambda, variables with coefficients equal to 0 are eliminated. (**C**) Receiver operating characteristic (ROC) curve of the diagnostic model (training set). (**D**) ROC curve of the diagnostic model (validation set).

3.5. Immune-related analyses of diagnostic genes

The bar charts illustrated the proportional distribution of 22 immune cell types across individual samples (Fig. 6A). Interestingly, four immune cell populations showed significant differences between AD and control group, such as B cells naive, M0 Macrophages, T cells follicular helper and gamma delta T cells (Fig. 6B). Further analysis revealed strong positive associations between all diagnostic genes and activated naive B cells dditionally, ARID5B exhibited a significant negative correlation with M0 macrophages (Fig. 6C).

3.6. The ceRNA regulatory network of diagnostic genes

Based on diagnostic genes, 88 co-mRNA-miRNA relationship pairs and 57 co-lncRNA-miRNA relationship pairs were identified (Fig. 7A and B). The lncRNA-miRNA-mRNA network included 2 diagnostic genes (ARID5B and SESN1), 7 miRNAs (hsa-miR-129-5p, hsa-miR-142-3p, hsa-miR-22-3p etc.), and 25 lncRNAs (PCGEM1, MALAT1, NEAT1, HCG18, DNAJC3-AS1, etc.) (Fig. 7C). The interactions delineated specific mRNA-miRNA pairings such as ARID5B-hsa-miR-129-5p and lncRNA-miRNA associations exemplified by FTX-hsa-miR-22-3p (**Additional file 7**).

3.7. Prediction of therapeutic agents of diagnostic genes

Using the Comparative Toxicogenomics Database (CTD), 33 therapeutic drugs were identified as targeting five diagnostic genes
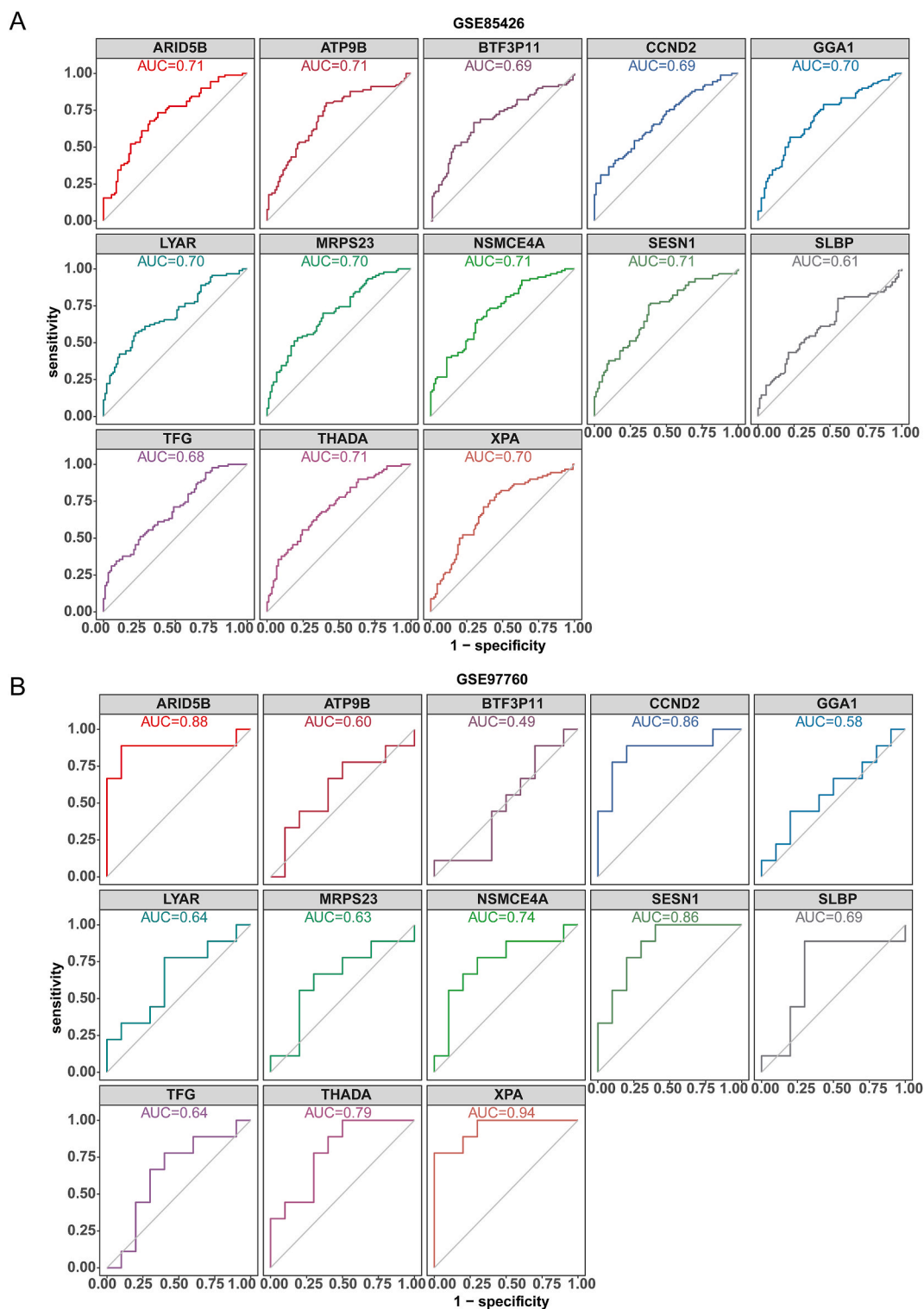
Fig. 4. ROC curve of key genes. (**A**) ROC curve of individual genes in the training set (GSE85426), and (**B**) ROC curve of individual genes in the validation set (GSE97760).

(Fig. 8). The network included 11 drugs for ARID5B (e.g., Valproic Acid, bisphenol A, sodium arsenite), 5 drugs for NSMCE4A (e.g., methylmercuric chloride, Ethinyl Estradiol), 18 drugs for SESN1 (e.g., Aflatoxin B1, Cyclosporine, Troglitazone), 7 drugs for THADA (e.g., cobaltous chloride, Acetaminophen, Methamphetamine), and 10 drugs for XPA (e.g., Tetrachlorodibenzodioxin, Benzo (a)
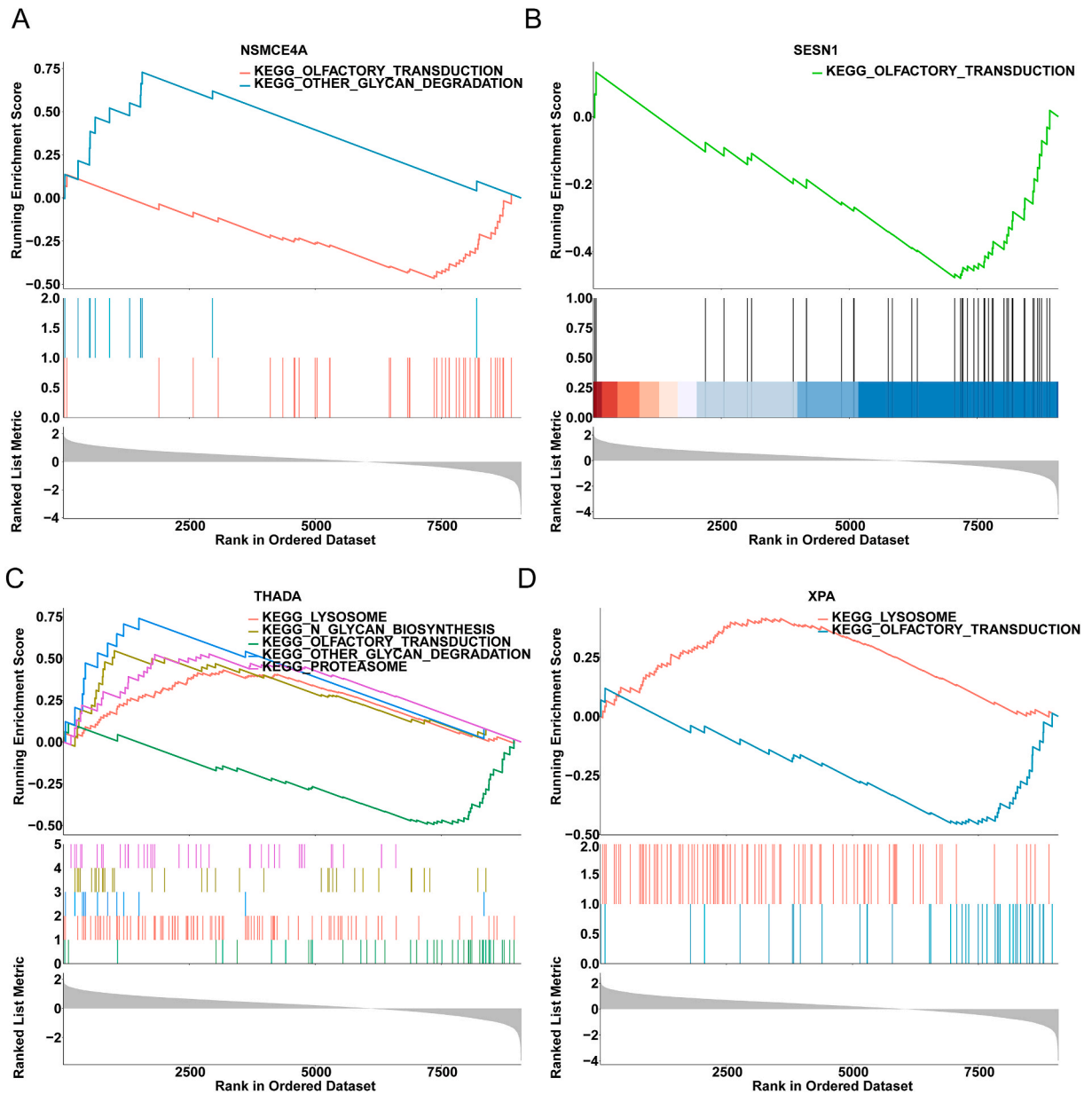
Fig. 5. Gene Set Enrichment Analysis. Enriched signaling pathways of (**A**) NSMCE4A, (**B**) SESN1, (**C**) THADA, (**D**) XPA. The top five lines in each figure represent the gene Enrichment Score's line graph. The vertical axis corresponds to the Running ES, and within the line graph is a peak. This peak represents the Enrichment score of this gene set, and the genes preceding this peak are the core genes under this gene set. The horizontal axis represents each gene within this gene set, corresponding to the barcode-like vertical lines in the second section.The second section: The barcode-like portion represents "Hits". Each vertical line corresponds to a gene under this gene set.The third section: This is the distribution graph of the rank values of all genes. The vertical axis represents the ranked list metric, indicating the rank value of that particular gene.

pyrene, methylmercuric chloride) (Fig. 8, Table 3).

3.8. The results of expression verification

In the training set (GSE85426), the expression levels of ARID5B, NSMCE4A, SESN1, THADA, and XPA are significantly higher in AD samples compared to control samples (Fig. 9A), indicating that these genes are upregulated. In the validation set (GSE97760), the expression trends of ARID5B, NSMCE4A, SESN1, and XPA are consistent with those observed in the training set (Fig. 9B). Additionally, significant differences in expression levels between AD and control samples are observed for ARID5B, SESN1, and XPA. Combining the data from Fig. 9A and B, it is evident that the expression levels of ARID5B, SESN1, and XPA are significantly higher in AD samples in

A

B

C
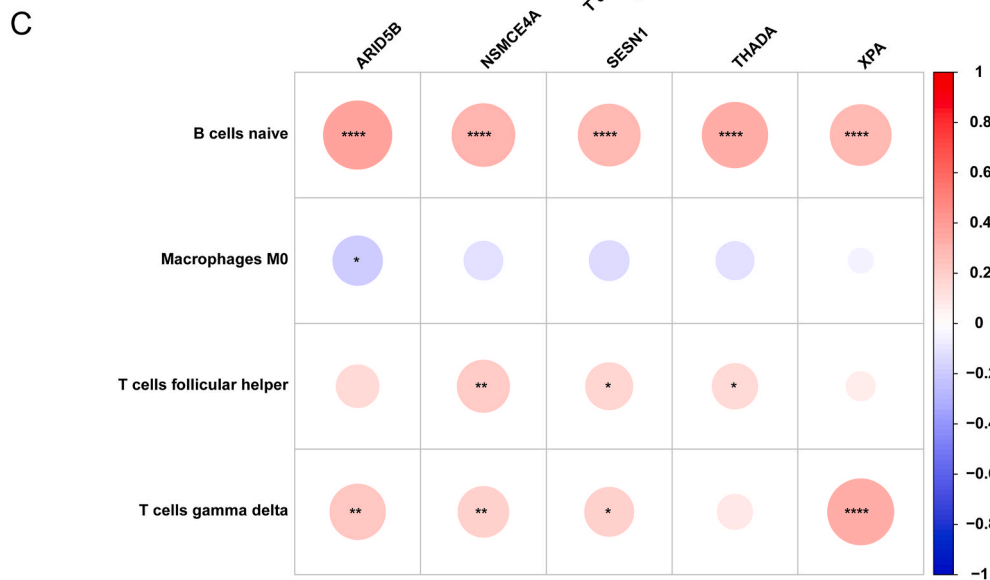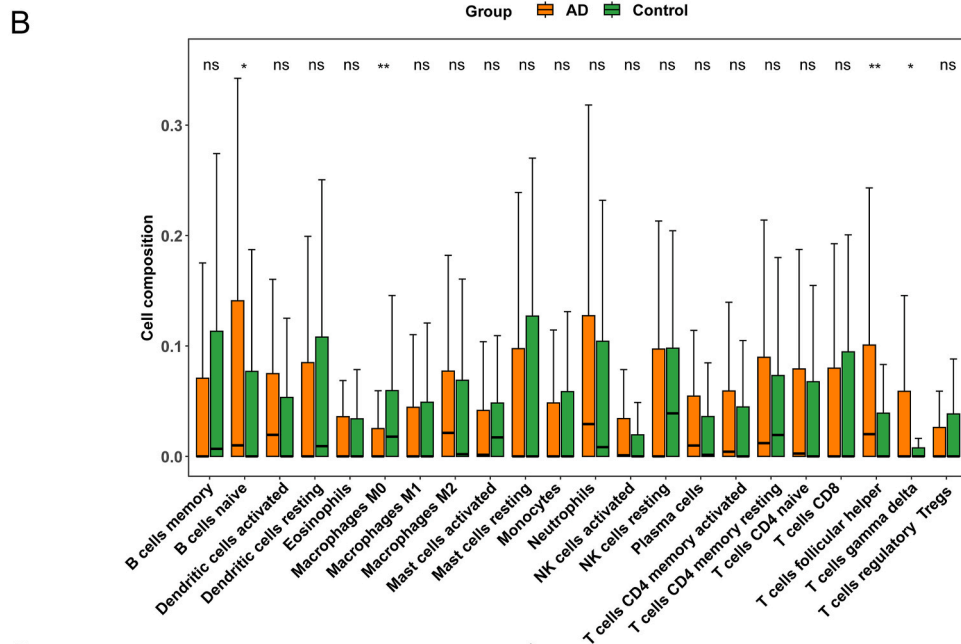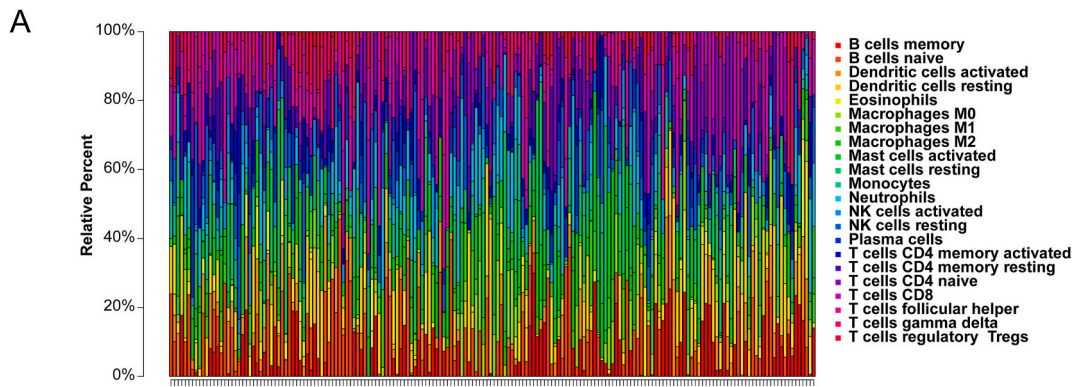
(caption on next page)

Fig. 6. Correlation between immune infiltration and diagnostic genes with differential immune cells. (**A**) Histogram of immune infiltration cell abundance. This bar chart visualizes the relative percentages of the 22 immune cells in each sample. Different colors represent different types of immune cells. (**B**) Box plot of the immune infiltration cell abundance between the AD and Control groups. 'ns' indicates p > 0.05 (not significant), '*' indicates p < 0.05, '**' indicates p < 0.01, '***' indicates p < 0.001, and '****' indicates p < 0.0001. (**C**) Heatmap of the correlation between differential immune infiltration cells and diagnostic genes. The larger the |r| value, the stronger the correlation. Red indicates a positive correlation, while blue indicates a negative correlation. (For interpretation of the references to color in this figure legend, the reader is referred to the Web version of this article.)
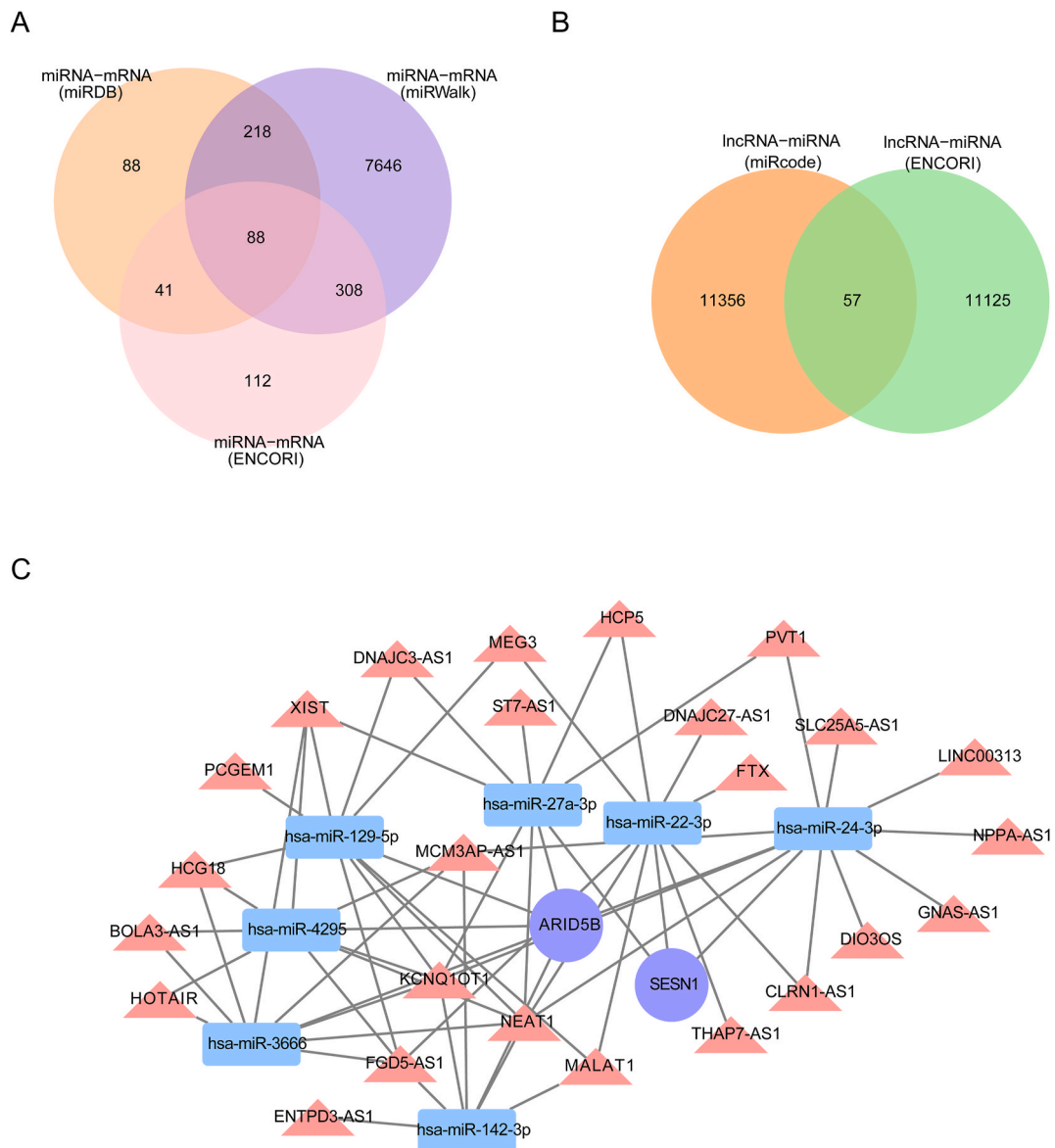

Fig. 7. The competing endogenous RNA (ceRNA) regulatory network of diagnostic genes. (**A**) Venn diagram of mRNA-miRNA relationship intersections. The orange represents the overlap between the miRDB database and diagnostic gene pairs. The purple represents the overlap of the miRWalk database with the diagnostic gene pairs. The pink represents the intersection of diagnostic genes and the ENCORI database relationship pairs. (**B**) Network of the intersection of miRNA-lncRNA relationship pairs. (**C**) The constructed lncRNA-miRNA-mRNA regulatory network, where the purple circles denote mRNA, blue rectangles represent miRNA, and red triangles symbolize lncRNA. (For interpretation of the references to color in this figure legend, the reader is referred to the Web version of this article.)
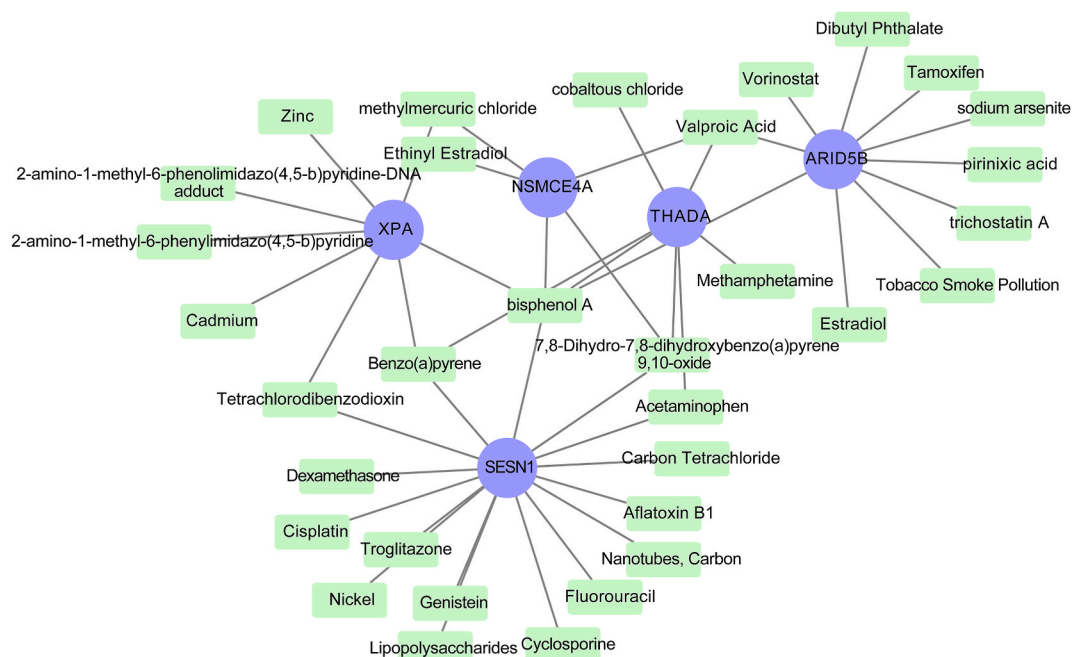
Fig. 8. Predicted mRNA-drug network. This figure visualizes the interaction between small molecule drugs and diagnostic genes. The purple circles represent diagnostic genes, while the green rectangles represent drugs. (For interpretation of the references to color in this figure legend, the reader is referred to the Web version of this article.)

both the training and validation sets. Therefore, ARID5B, SESN1, and XPA can be considered biomarkers for this study.

3.9. Immunohistochemistry of the CA1 region of mouse hippocampus

Immunohistochemical analyses of paraffin-embedded mouse brain sections revealed that expression levels of Aβ and Caspase-3 in the hippocampal CA1 region of APP/PS1 mice were markedly elevated compared to their WT littermates. (Fig. 10A–B). APP/PS1 mice are commonly used as a transgenic model in AD research. The mouse genome has been modified to overexpress human mutant APP (amyloid precursor protein) and PS1 (presenilin 1) genes associated with early-onset AD, leading to increased production and accumulation of Aβ in the mouse brain. Caspase-3, an essential apoptotic executioner enzyme, plays a central role in the cell apoptosis pathway. This neuronal cell apoptosis contributes to further cognitive impairment in APP/PS1 mice.

3.10. Results of Western blot and qPCR analysis of mouse brain

Western blotting and quantitative PCR analyses revealed elevated protein and mRNA expression levels of ARID5B, XPA, and SESN1 in the cerebral tissues of APP/PS1 mice, surpassing those observed in the WT cohort (Fig. 11A–I). These findings are consistent with previous gene expression level validations.

4. Discussion

AD is the leading cause of dementia, imposing a significant medical burden and associated costs. Two primary hypotheses for the cause of AD are the cholinergic hypothesis and the amyloid hypothesis, with symptoms worsening with age [28]. Clinical interventions targeting AD pathology have so far produced suboptimal outcomes, likely due to late-stage intervention. Therefore, the exploration of early diagnostic markers for AD is crucial [29,30]. Evidence suggests that lactic acid may serve as an alternative energy substrate, mitigating neuronal energy deficits and providing neuroprotection [31,32]. Elevated levels of lactic acid have been observed in the cerebrospinal fluid and post-mortem brain tissue of patients with AD [9,10]. Moreover, intravenous sodium lactate infusion in AD patients do not change their cognitive impairment [33]. Therefore, it is highly probable that the increase in brain lactic acid may exacerbate the cognitive impairment in AD patients. However, research on the mechanisms related to histone lactylation in AD is limited. This study utilized bioinformatics techniques to explore the biological processes involving HLRGs in AD and developed diagnostic biomarkers based on HLRGs. This work provides a theoretical foundation for advancing the understanding of AD pathogenesis and refining diagnostic and therapeutic approaches.

Our KEGG pathway enrichment analysis indicates significant enrichment in pathways such as Cellular senescence, Cell cycle, and Basal transcription factors. GSEA results show that the genes XPA and SESN1 are enriched in the olfactory transduction pathway, with

Table 3
Lists of the small molecule drugs corresponding to the five diagnostic genes.

Gene	Chemical	Reference Count	Gene	Chemical	Reference Count
ARID5B	Valproic Acid	6	SESN1	Carbon Tetrachloride	2
ARID5B	bisphenol A	4	SESN1	bisphenol A	2
ARID5B	sodium arsenite	2	SESN1	Tetrachlorodibenzodioxin	2
ARID5B	Valproic Acid	2	SESN1	Nickel	2
ARID5B	Tamoxifen	2	SESN1	bisphenol A	2
ARID5B	Estradiol	2	SESN1	7,8-Dihydro-7,8-dihydroxyben zo(a)pyrene 9,10-oxide	2
ARID5B	Vorinostat	2	SESN1	Nanotubes, Carbon	2
ARID5B	Tobacco Smoke Pollution	2	SESN1	Fluorouracil	2
ARID5B	Dibutyl Phthalate	2	THADA	Benzo(a)pyrene	5
ARID5B	trichostatin A	2	THADA	bisphenol A	3
ARID5B	pirinixic acid	2	THADA	cobaltous chloride	2
NSMCE4 A	Valproic Acid	3	THADA	Acetaminophen	2
NSMCE4 A	bisphenol A	2	THADA	Methamphetamine	2
NSMCE4 A	methylmercuric chloride	2	THADA	Valproic Acid	2
NSMCE4 A	7,8-Dihydro-7,8-d ihydroxybenzo(a) pyrene 9,10-oxide	2	THADA	7,8-Dihydro-7,8-dihydroxyben zo(a)pyrene 9,10-oxide	2
NSMCE4 A	Ethinyl Estradiol	2	XPA	Zinc	3
SESN1	Benzo(a)pyrene	6	XPA	2-amino-1-methyl-6-phenylimi dazo (4,5-b)pyridine	3
SESN1	Tetrachlorodibenz odioxin	5	XPA	bisphenol A	2
SESN1	Cisplatin	5	XPA	Tetrachlorodibenzodioxin	2
SESN1	Aflatoxin B1	4	XPA	Benzo(a)pyrene	2
SESN1	Cyclosporine	3	XPA	methylmercuric chloride	2
SESN1	Troglitazone	3	XPA	Cadmium	2
SESN1	Dexamethasone	3	XPA	2-amino-1-methyl-6-phenolimi dazo (4,5-b) pyridine-DNA adduct	2
SESN1	Acetaminophen	3	XPA	Benzo(a)pyrene	2
SESN1	Lipopolysacc ari des	2	XPA	bisphenol A	2
SESN1	Genistein	2			

Small molecule drugs predicted for diagnostic genes are retained based on the screening criterion of Reference Count >1.

XPA also enriched in the lysosome pathway. Aging is identified as the primary risk factor for AD [34], with neuronal cell senescence being a key contributor to brain aging in AD. Although not definitively causal or consequential, substantial evidence suggests a strong association between cellular senescence and AD [35]. Numerous studies have identified a range of factors that induce cellular senescence, including telomere attrition, compromised mitochondrial function, genomic instability, oncogenic stimuli, inflammatory responses, and metabolic disturbances [36]. It is hypothesized that XPA may mitigate cellular senescence by facilitating DNA repair, thereby delaying AD progression. SESN1 is associated with cellular senescence under various conditions and may regulate the elimination of senescent cells through its effects on low-grade inflammation (SCLGI), thus slowing AD progression [37]. Interestingly, GSEA analysis shows that XPA is related to lysosomes, and many studies indicate that lysosomes can improve β-amyloid precursor protein and Tau pathology in AD models [38].

ARID5B belongs to the AT-rich interactive domain-containing protein family, known for its affinity for AT-rich regions in double-stranded DNA [39]. The ARID5B is involved in orchestrating gene expression crucial for adipogenesis and hepatic morphogenesis, influencing the proliferation and maturation of B lymphocyte progenitors. Additionally, polymorphic variations in this gene have been linked to increased susceptibility to acute lymphoblastic leukemia, highlighting its role in cellular development and pathogenesis [40]. In recent years, ARID5B has also been associated with glucose metabolism. The glucose oxidation rate in ARID5B knockout (Arid5b −/−) mice is significantly higher than in WT mice, and the lactic acid content of the anaerobic glycolysis end product in Arid5b −/− mice is lower than in WT mice [41]. However, the mechanism of ARID5B in AD remains unclear. For the first time, this study suggests that ARID5B may be related to AD. ARID5B is involved in the regulation of gene transcription and expression [42], potentially playing a significant role in the early stages of AD. Early AD primarily involves neuronal damage and synaptic dysfunction [43], hence, ARID5B might influence AD development by regulating genes associated with neuronal function and synaptic connectivity. This may be related to ARID5B's connection with glucose metabolism. Elevated expression of ARID5B is associated with the pathogenesis of AD, potentially leading to an imbalance in lactate accumulation within brain tissues.

Xeroderma pigmentosum (XP) is a rare genetic disorder characterized by autosomal recessive inheritance, primarily affecting the cellular DNA repair machinery. Xeroderma pigmentosum group A (XPA) was the first disorder identified as resulting from defective DNA repair mechanisms. XPA patients often experience varying degrees of neurodegeneration [44,45]. XPA plays a crucial role in the nucleotide excision repair (NER) pathway, essential for maintaining DNA integrity [46]. The NER mechanism divides into two distinct pathways: global-genomic nucleotide excision repair (GG-NER), which operates across the entire genome, and transcription-coupled
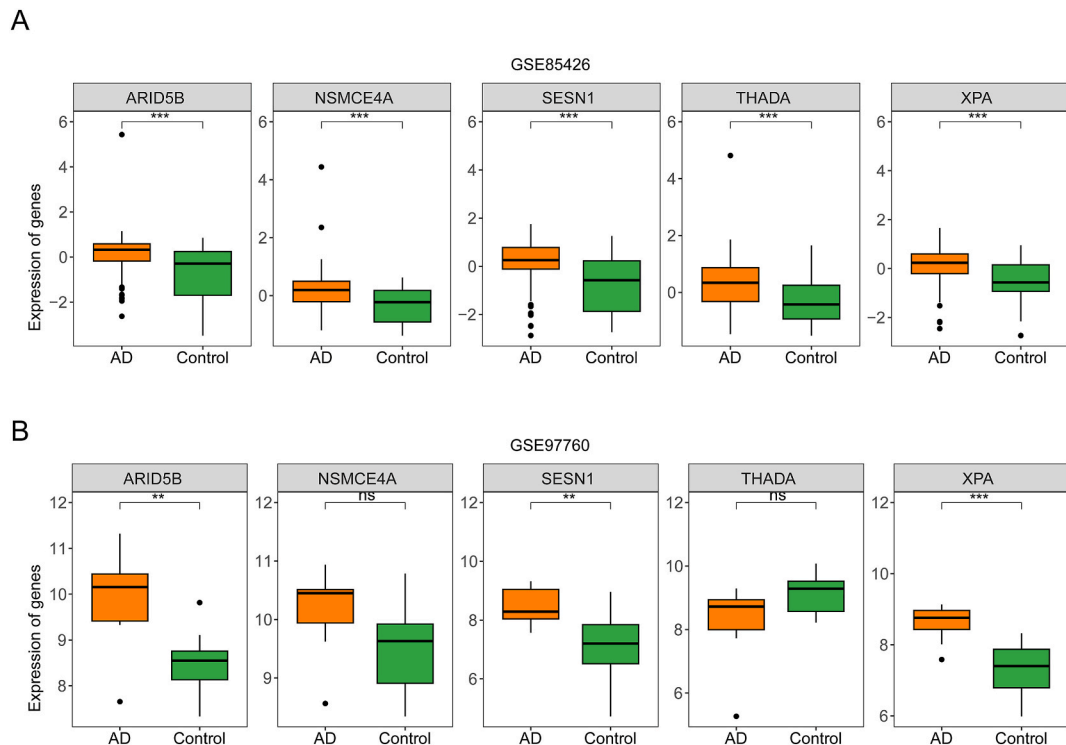
A

B

Fig. 9. Box plot of gene expression levels. (**A**) Box plot of the expression levels of genes ARID5B, NSMCE4A, SESN1, THADA, XPA in the training set (GSE85426). (**B**) Box plot of the expression levels of the same genes in the validation set (GSE97760).
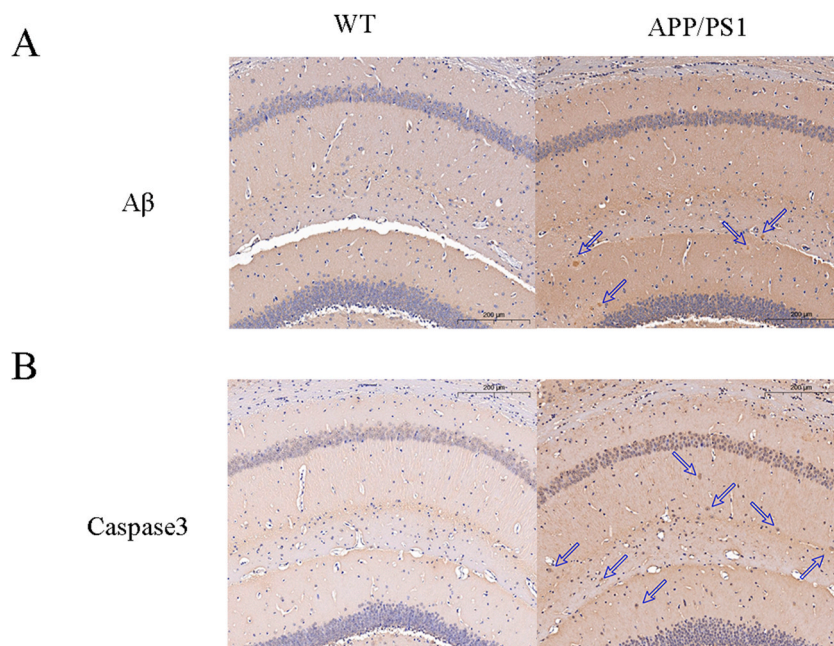

Fig. 10. Immunohistochemistry of the mouse hippocampal CA1 region. (A) The arrows indicate the deposition of Aβ in the hippocampal CA1 region. The left image is from a WT mouse, while the right image is from an 8-month-old APP/PS1 mouse. (B) The arrows point to the deposition of Caspase3 in the hippocampal CA1 region of mice, where the left image is from a WT mouse and the right image is from an APP/PS1 mouse. The sample size is n = 3. The scale bar is 200 μm. The magnification is 20×.
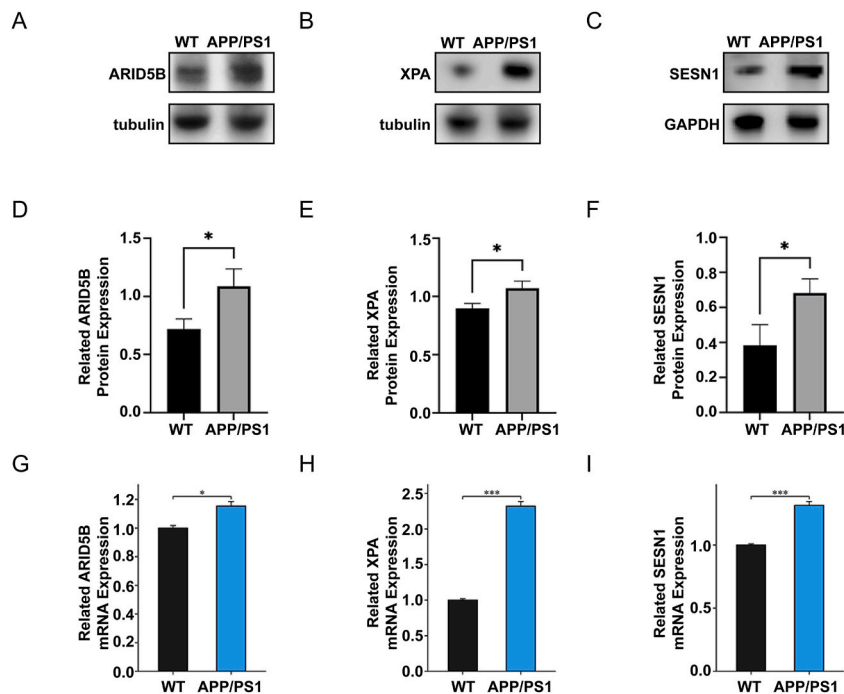
Fig. 11. Western blot and qPCR experimental results of mouse brain. Protein expression image and statistic value of (**A-B**) ARID5B ($P < 0.05$), (**C-D**) XPA ($P < 0.05$), and (**E-F**) SESN1 ($P < 0.05$), n = 3. Bars represent mean ± SEM. The mRNA expression levels of (**G**) ARID5B ($P < 0.05$), (**H**) XPA ($P < 0.001$), and (**I**) SESN1 ($P < 0.001$) were measured by qPCR, n = 3. Bars represent mean ± SEM.

nucleotide excision repair (TC-NER), which specifically addresses lesions obstructing transcriptional processes [47]. XPA mainly functions in TC-NER, acting as a translocase and helicase to unwind DNA [48], then using two nucleases, XPF and XPG, to excise DNA damage through double DNA cuts, filling the gap with Polδ/ε and ligase I [47]. Changes in DNA damage and DNA repair ability may be closely related to AD [49]. Deficiencies in DNA repair can lead to cellular depletion of nicotinamide adenine dinucleotide (NAD+), impacting mitochondrial autophagy, resulting in the accumulation of damaged mitochondria, metabolic disorders, energy deficiency, and ultimately, neurological deficits. These phenotypes parallel those observed in AD [50]. While the Base Excision Repair (BER) pathway is considered the primary DNA damage rectification mechanism in AD [51], NER also participates in DNA damage repair in AD [52]. The XP family, including XPA, XPB, XPF, and XPG, is widely involved in the NER repair pathway and is implicated in neurodegeneration [53]. Therefore, as a key gene in the DNA damage repair pathway, XPA may serve as a potential diagnostic marker for AD. XPA may play a role in the early stages of AD by promoting DNA repair to protect neurons from damage. However, in the middle and late stages of the disease, as neurodegeneration intensifies and neuronal loss occurs, DNA repair mechanisms may become less effective, diminishing the impact of XPA during these advanced stages.

Sestrins (SESN) are a highly conserved, stress-induced protein family involved in various biological processes, comprising SESN1, SESN2, and SESN3. Sestrin1 (SESN1) is a prominent neuroprotective protein. Upregulated SESN1 protein can reduce intracellular ROS accumulation and improve neuronal damage by downregulating Kelch-like ECH-associated protein 1 (Keap1), thereby promoting the activity of nuclear factor erythroid 2-related factor 2 (Nrf2) [54]. SESN1 is directly regulated by P53, which reduces oxidative stress-induced DNA damage by regulating SESN1 expression [55,56]. A substantial body of research has linked age-associated disorders, such as AD, to the progressive accrual of oxidative stress [57]. With its antioxidant and DNA repair functions, SESN1 may play a neuroprotective role in AD, making it a potential pathological marker for the disease. During the middle and late stages of AD, oxidative stress and cell apoptosis become primary pathological processes. Thus, SESN1 could influence disease progression in these stages by regulating oxidative stress and cell death pathways. Additionally, SESN1 has been associated with neurodegeneration and brain injury [54], which are characteristic of the middle and late stages of AD.

Using the CIBERSORT algorithm, the differences in immune cell infiltration between patients with AD and controls were assessed through gene expression profiles. Spearman correlation analysis was conducted to discern the relationships between diverse immune infiltrates and diagnostic genes. The results indicated that ARID5B, NSMCE4A, SESN1, THADA, and XPA are all significantly correlated with naive B cells. Naive B cells, which have not been exposed to antigens, play a crucial role in the immune system. Upon encountering antigens, naive B cells can differentiate into plasma cells that produce antibodies or memory B cells that can "remember" antigens and respond more rapidly upon re-exposure [58]. B cells can produce antibodies that aid in the clearance of β-amyloid protein, but they may also exacerbate neuroinflammation [59]. While current research does not fully elucidate the connection between B cells and AD, further investigation is necessary to better understand and apply this relationship. Diagnosing early AD is challenging, and the sensitivity of miRNAs in early stages suggests they could serve as potential disease markers [60]. Ou et al. constructed an

AD-related ceRNA network including two lncRNAs (NEAT1 and MIAT), three miRNAs (hsa-miR-551a, hsa-miR-133b, and hsa-miR-206), and two mRNAs (CXCR4 and GNG3). It provided a new reference for the treatment of AD [61].

Constructing a competing endogenous RNA (ceRNA) network can elucidate the relationships between various non-coding RNAs and five target genes (ARID5B, NSMCE4A, SESN1, THADA, XPA). This ceRNA network may reveal novel targets for AD therapeutics and provide new biomarkers for diagnosis. The lncRNA-miRNA-mRNA regulatory network identified 2 mRNAs, 7 miRNAs, and 25 lncRNAs. Notably, miR-22-3p and miR-24-3p are downregulated in the cerebrospinal fluid of individuals with AD, with miR-22-3p primarily involved in the MAPK pathway. Impairment of the MAPK pathway can lead to AD [62,63]. Additionally, miR-27a-3p, downregulated in the serum and cerebrospinal fluid of patients with AD, is positively correlated with BACE1, a key enzyme for $A\beta$ synthesis. The specific regulatory mechanism of miR-27a-3p on BACE1 remains unexplored. ATG16L1, regulated by miR-142-3p, is a key gene for autophagy [64], with dysregulated autophagy increasingly recognized as a contributing factor to AD pathogenesis [65]. Diagnosing early AD is challenging, and the sensitivity of miRNAs in early stages suggests they could serve as potential disease markers [60]. Ou et al. constructed an AD-related ceRNA network including two lncRNAs (NEAT1 and MIAT), three miRNAs (hsa-miR-551a, hsa-miR-133b, and hsa-miR-206), and two mRNAs (CXCR4 and GNG3). It provided a new reference for the treatment of AD [61].

Gene-drug network analysis identified several drugs with potential therapeutic value for AD. Troglitazone, a PPARgamma agonist, can alleviate $A\beta$-induced hippocampal LTP damage in rats [66] and mediates cyclin-dependent kinase 5 inhibition in SH-SY5Y neuroblastoma cells, reducing tau phosphorylation [67]. Acetaminophen, a widely used non-prescription drug for its antipyretic and analgesic properties, has been shown in vitro to reduce neuronal death caused by Menadione treatment [68] and alleviate oxidative stress in PC12 and hippocampal neurons treated with amyloid beta-peptides [69]. Valproic acid exhibits neuroprotective effects in AD, reducing $A\beta$ deposition and improving memory deficits in AD model mice, making it a promising drug for targeting AD [70,71]. Vorinostat, an HDAC inhibitor, also demonstrates neuroprotective effects in AD model mice [72]. Four drugs identified with potential for AD treatment are Troglitazone, Acetaminophen, Valproic acid, and Vorinostat. However, these drugs have only shown some success in in vitro or animal studies and still require extensive clinical trials and safety assessments.

This study has several limitations that should be acknowledged. We used only the APP/PS1 mouse model to investigate Alzheimer's disease (AD). While this model is valuable for replicating certain pathological features of AD, it does not fully capture the complexity of the human condition. Relying solely on a single animal model may limit our understanding of how these biomarkers behave under different AD pathological states. Future studies should incorporate a variety of models and larger sample sizes to better validate the relevance and specificity of these biomarkers. Our sample size in each group was relatively small, with only 10 samples in both the APP/PS1 and WT groups. Although this number is sufficient for an initial investigation, it may limit the statistical power and generalizability of the findings. Additionally, the protein expression level of the biomarker SESN1 was low, resulting in overexpression in the Western blot analysis. This technical limitation may affect the accuracy of protein level assessments and introduce bias in the interpretation of the results. Future studies should consider using more sensitive detection techniques or optimizing sample processing methods to mitigate this issue. Although our bioinformatics analysis identified ARID5B, SESN1, and XPA as potential diagnostic biomarkers for AD, their clinical applicability still needs to be validated in larger cohorts and more comprehensive studies. Further research is also needed to elucidate the potential mechanisms by which these genes influence AD pathology and to confirm their value in clinical settings.

5. Conclusion

Bioinformatics and animal studies identified three genes, ARID5B, SESN1, and XPA, as biomarkers. SESN1 and XPA may influence AD development by affecting cellular senescence and cell cycle pathways. Additionally, XPA could improve β-amyloid precursor protein and Tau pathology via the lysosomal pathway. Potential AD drugs identified include Troglitazone, Acetaminophen, Valproic acid, and Vorinostat. These biomarkers offer valuable insights into further AD research.

Ethics approval and consent to participate

The Nanjing University of Chinese Medicine's Animal Care and Use Committee sanctioned all animal-related study protocols. Approval Number: A220601. Experimental procedures on animals adhered strictly to the ARRIVE guidelines and conformed with the U.K. Animals (Scientific Procedures) Act, 1986, alongside related guidelines and the EU Directive 2010/63/EU governing animal experimentation.

Consent for publication

Not applicable.

Funding

Data availability statement

The datasets underpinning the analyses of this study are accessible within the GEO repositories [https://www.ncbi.nlm.nih.gov/geo/], specifically under the accession numbers GSE85426 and GSE97760.The study's primary findings are detailed within the manuscript and its accompanying Supplementary Information. Correspondence regarding this research should be addressed to the corresponding author.

CRediT authorship contribution statement

Shaobo Guo: Writing – review & editing, Writing – original draft, Visualization, Validation, Methodology, Formal analysis, Conceptualization. **Wenhui Zhu:** Validation, Formal analysis, Data curation. **Yuting Bian:** Methodology, Formal analysis. **Zhikai Li:** Writing – review & editing, Writing – original draft. **Heng Zheng:** Visualization, Software, Formal analysis. **Wenlong Li:** Formal analysis, Data curation. **Yi Yang:** Software, Investigation, Formal analysis, Conceptualization. **Xuzheng Ji:** Visualization, Validation. **Biao Zhang:** Writing – review & editing, Resources, Conceptualization.

Declaration of competing interest

The authors assert the nonexistence of any competing financial or personal interests pertaining to this manuscript.

Abbreviations

APP/PS1   APPswe/PSEN1dE9
ARID5B   AT-rich interaction domain 5B
AUC   area under the curve
BER   Base excision repair
ceRNA   competing endogenous RNA
DEGs   differentially expressed genes
GO   Gene Ontology
GSEA   gene set enrichment analysis
HDAC   Histone deacetylases
HLRGS   Histone lactylation-related genes
KEGG   Kyoto Encyclopedia of Genes and Genomes
LASSO   least absolute shrinkage and selection operator
NAD^+ Consumption of nicotinamide adenine dinucleotide
NER   Nucleotide excision repair
Nrf2   Uclear factor erythroid 2-related factor 2
PPI   protein-protein interactions
qRT-PCR   quantitative real-time Polymerase Chain Reaction
ROC   Receiver operating characteristic
SCLGI   Low-grade inflammation
SESN1   Sestrin 1
WT   Wild-type littermates
XPA   Xeroderma pigmentosum, complementation group A

Appendix A. Supplementary data

Supplementary data to this article can be found online at https://doi.org/10.1016/j.heliyon.2024.e37807.

References

[1] P. Scheltens, B. De Strooper, M. Kivipelto, H. Holstege, G. Chételat, C.E. Teunissen, J. Cummings, van der Flier WM: Alzheimer's disease, Lancet 397 (10284) (2021) 1577–1590, https://doi.org/10.1016/s0140-6736(20)32205-4.
[2] Christina P: World Alzheimer Report 2018.the State of the Art of Dementia Research: New Frontiers. Alzheimer's Disease International, London. .doi: https://doi.org/APO-260056.
[3] A. Europe, Dementia in europe yearbook 2019: estimating the prevalence of dementia in europe, Alzheimer Europe 180 (2019).
[4] J.L. Cummings, T. Morstorf, K. Zhong, Alzheimer's disease drug-development pipeline: few candidates, frequent failures, Alzheimer's Res. Ther. 6 (4) (2014) 37, https://doi.org/10.1186/alzrt269.
[5] Perkovic M. Nikolac, A. Videtic Paska, M. Konjevod, K. Kouter, D. Svob Strac, G. Nedic Erjavec, N. Pivac, Epigenetics of alzheimer's disease, Biomolecules 11 (2) (2021), https://doi.org/10.3390/biom11020195.
[6] D. Zhang, Z. Tang, H. Huang, G. Zhou, C. Cui, Y. Weng, W. Liu, S. Kim, S. Lee, M. Perez-Neut, J. Ding, D. Czyz, R. Hu, Z. Ye, M. He, et al., Metabolic regulation of gene expression by histone lactylation, Nature 574 (7779) (2019) 575–580, https://doi.org/10.1038/s41586-019-1678-1.

[7] R.A. Harris, L. Tindale, A. Lone, O. Singh, S.L. Macauley, M. Stanley, D.M. Holtzman, R. Bartha, R.C. Cumming, Aerobic glycolysis in the frontal cortex correlates with memory performance in wild-type mice but not the APP/PS1 mouse model of cerebral amyloidosis, J. Neurosci. 36 (6) (2016) 1871–1878, https://doi.org/10.1523/jneurosci.3131-15.2016.

[8] K.E. Weaver, T.L. Richards, R.G. Logsdon, E.L. McGough, S. Minoshima, E.H. Aylward, N.M. Kleinhans, T.J. Grabowski, S.M. McCurry, L. Teri, Posterior cingulate lactate as a metabolic biomarker in amnestic mild cognitive impairment, BioMed Res. Int. 2015 (2015) 610605, https://doi.org/10.1155/2015/610605.

[9] C. Liguori, A. Stefani, G. Sancesario, G.M. Sancesario, M.G. Marciani, M. Pierantozzi, CSF lactate levels, τ proteins, cognitive decline: a dynamic relationship in Alzheimer's disease, J. Neurol. Neurosurg. Psychiatry 86 (6) (2015) 655–659, https://doi.org/10.1136/jnnp-2014-308577.

[10] R.Y. Pan, L. He, J. Zhang, X. Liu, Y. Liao, J. Gao, Y. Liao, Y. Yan, Q. Li, X. Zhou, J. Cheng, Q. Xing, F. Guan, J. Zhang, L. Sun, et al., Positive feedback regulation of microglial glucose metabolism by histone H4 lysine 12 lactylation in Alzheimer's disease, Cell Metab 34 (4) (2022) 634–648.e636, https://doi.org/10.1016/j.cmet.2022.02.013.

[11] P.C. Pao, D. Patnaik, L.A. Watson, F. Gao, L. Pan, J. Wang, C. Adaikkan, J. Penney, H.P. Cam, W.C. Huang, L. Pantano, A. Lee, A. Nott, T.X. Phan, E. Gjoneska, et al., HDAC1 modulates OGG1-initiated oxidative DNA damage repair in the aging brain and Alzheimer's disease, Nat. Commun. 11 (1) (2020) 2484, https://doi.org/10.1038/s41467-020-16361-y.

[12] M.M. Dobbin, R. Madabhushi, L. Pan, Y. Chen, D. Kim, J. Gao, B. Ahanonu, P.C. Pao, Y. Qiu, Y. Zhao, L.H. Tsai, SIRT1 collaborates with ATM and HDAC1 to maintain genomic stability in neurons, Nat. Neurosci. 16 (8) (2013) 1008–1015, https://doi.org/10.1038/nn.3460.

[13] J.S. Guan, S.J. Haggarty, E. Giacometti, J.H. Dannenberg, N. Joseph, J. Gao, T.J. Nieland, Y. Zhou, X. Wang, R. Mazitschek, J.E. Bradner, R.A. DePinho, R. Jaenisch, L.H. Tsai, HDAC2 negatively regulates memory formation and synaptic plasticity, Nature 459 (7243) (2009) 55–60, https://doi.org/10.1038/nature07925.

[14] J. Gräff, D. Rei, J.S. Guan, W.Y. Wang, J. Seo, K.M. Hennig, T.J. Nieland, D.M. Fass, P.F. Kao, M. Kahn, S.C. Su, A. Samiei, N. Joseph, S.J. Haggarty, I. Delalle, et al., An epigenetic blockade of cognitive functions in the neurodegenerating brain, Nature 483 (7388) (2012) 222–226, https://doi.org/10.1038/nature10849.

[15] C. Moreno-Yruela, D. Zhang, W. Wei, M. Bæk, W. Liu, J. Gao, D. Danková, A.L. Nielsen, J.E. Bolding, L. Yang, S.T. Jameson, J. Wong, C.A. Olsen, Y. Zhao, Class I histone deacetylases (HDAC1-3) are histone lysine delactylases, Sci. Adv. 8 (3) (2022) eabi6696, https://doi.org/10.1126/sciadv.abi6696.

[16] M. Kilgore, C.A. Miller, D.M. Fass, K.M. Hennig, S.J. Haggarty, J.D. Sweatt, G. Rumbaugh, Inhibitors of class 1 histone deacetylases reverse contextual memory deficits in a mouse model of Alzheimer's disease, Neuropsychopharmacology 35 (4) (2010) 870–880, https://doi.org/10.1038/npp.2009.197.

[17] Y. Han, L. Chen, J. Liu, J. Chen, C. Wang, Y. Guo, X. Yu, C. Zhang, H. Chu, H. Ma, A class I HDAC inhibitor rescues synaptic damage and neuron loss in APP-transfected cells and APP/PS1 mice through the GRIP1/AMPA pathway, Molecules 27 (13) (2022), https://doi.org/10.3390/molecules27134160.

[18] N. Wang, W. Wang, X. Wang, G. Mang, J. Chen, X. Yan, Z. Tong, Q. Yang, M. Wang, L. Chen, P. Sun, Y. Yang, J. Cui, M. Yang, Y. Zhang, et al., Histone lactylation boosts reparative gene activation post-myocardial infarction, Circ. Res. 131 (11) (2022) 893–908, https://doi.org/10.1161/circresaha.122.320488.

[19] M.E. Ritchie, B. Phipson, D. Wu, Y. Hu, C.W. Law, W. Shi, G.K. Smyth, Limma powers differential expression analyses for RNA-sequencing and microarray studies, Nucleic acids research 43 (7) (2015) e47, https://doi.org/10.1093/nar/gkv007.

[20] K. Ito, D. Murphy, Application of ggplot2 to pharmacometric graphics, CPT Pharmacometrics Syst. Pharmacol. 2 (10) (2013) e79, https://doi.org/10.1038/psp.2013.56.

[21] M.R. Ferreira, G.A. Santos, C.A. Biagi, W.A. Silva Junior, W.F. Zambuzzi, GSVA score reveals molecular signatures from transcriptomes for biomaterials comparison, J. Biomed. Mater. Res. 109 (6) (2021) 1004–1014, https://doi.org/10.1002/jbm.a.37090.

[22] P. Langfelder, S. Horvath, WGCNA: an R package for weighted correlation network analysis, BMC Bioinf. 9 (2008) 559, https://doi.org/10.1186/1471-2105-9-559.

[23] T. Wu, E. Hu, S. Xu, M. Chen, P. Guo, Z. Dai, T. Feng, L. Zhou, W. Tang, L. Zhan, X. Fu, S. Liu, X. Bo, G. Yu, clusterProfiler 4.0: a universal enrichment tool for interpreting omics data, Innovation 2 (3) (2021) 100141, https://doi.org/10.1016/j.xinn.2021.100141.

[24] J. Friedman, T. Hastie, R. Tibshirani, Regularization paths for generalized linear models via coordinate descent, J Stat Softw 33 (1) (2010) 1–22.

[25] X. Robin, N. Turck, A. Hainard, N. Tiberti, F. Lisacek, J.C. Sanchez, M. Müller, pROC: an open-source package for R and S+ to analyze and compare ROC curves, BMC Bioinf. 12 (2011) 77, https://doi.org/10.1186/1471-2105-12-77.

[26] A.M. Newman, C.L. Liu, M.R. Green, A.J. Gentles, W. Feng, Y. Xu, C.D. Hoang, M. Diehn, A.A. Alizadeh, Robust enumeration of cell subsets from tissue expression profiles, Nat. Methods 12 (5) (2015) 453–457, https://doi.org/10.1038/nmeth.3337.

[27] G. Su, J.H. Morris, B. Demchak, G.D. Bader, Biological network exploration with Cytoscape 3, Curr Protoc Bioinformatics 47 (8.13) (2014) 11–24, https://doi.org/10.1002/0471250953.bi0813s47.

[28] Z. Breijyeh, R. Karaman, Comprehensive review on alzheimer's disease: causes and treatment, Molecules 25 (24) (2020), https://doi.org/10.3390/molecules25245789.

[29] R.A. Sperling, CR. Jr. Jack, Aisen PS: testing the right target and right drug at the right stage, Sci. Transl. Med. 3 (111) (2011) 111cm133, https://doi.org/10.1126/scitranslmed.3002609.

[30] P.S. Aisen, G.A. Jimenez-Maggiora, M.S. Rafii, S. Walter, R. Raman, Early-stage Alzheimer disease: getting trial-ready, Nat. Rev. Neurol. 18 (7) (2022) 389–399, https://doi.org/10.1038/s41582-022-00645-6.

[31] A. Atlante, L. de Bari, A. Bobba, G. Amadoro, A disease with a sweet tooth: exploring the Warburg effect in Alzheimer's disease, Biogerontology 18 (3) (2017) 301–319, https://doi.org/10.1007/s10522-017-9692-x.

[32] M. Zhang, X. Cheng, R. Dang, W. Zhang, J. Zhang, Z. Yao, Lactate deficit in an alzheimer disease mouse model: the relationship with neuronal damage, J. Neuropathol. Exp. Neurol. 77 (12) (2018) 1163–1176, https://doi.org/10.1093/jnen/nly102.

[33] J. Kálmán, A. Palotás, G. Kis, K. Boda, P. Túri, F. Bari, F. Domoki, I. Dóda, M. Argyelán, G. Vincze, T. Séra, L. Csernay, Z. Janka, L. Pávics, Regional cortical blood flow changes following sodium lactate infusion in Alzheimer's disease, Eur. J. Neurosci. 21 (6) (2005) 1671–1678, https://doi.org/10.1111/j.1460-9568.2005.03924.x.

[34] Z. Li, Z. Zhang, Y. Ren, Y. Wang, J. Fang, H. Yue, S. Ma, F. Guan, Aging and age-related diseases: from mechanisms to therapeutic strategies, Biogerontology 22 (2) (2021) 165–187, https://doi.org/10.1007/s10522-021-09910-5.

[35] S. Saez-Atienzar, E. Masliah, Cellular senescence and Alzheimer disease: the egg and the chicken scenario, Nat. Rev. Neurosci. 21 (8) (2020) 433–444, https://doi.org/10.1038/s41583-020-0325-z.

[36] Z. Si, L. Sun, X. Wang, Evidence and perspectives of cell senescence in neurodegenerative diseases, Biomed. Pharmacother. 137 (2021) 111327, https://doi.org/10.1016/j.biopha.2021.111327.

[37] G. Livshits, A. Kalinkovich, A cross-talk between sestrins, chronic inflammation and cellular senescence governs the development of age-associated sarcopenia and obesity, Ageing Res. Rev. 86 (2023) 101852, https://doi.org/10.1016/j.arr.2023.101852.

[38] J.X. Song, S. Malampati, Y. Zeng, S.S.K. Durairajan, C.B. Yang, B.C. Tong, A. Iyaswamy, W.B. Shang, S.G. Sreenivasmurthy, Z. Zhu, K.H. Cheung, J.H. Lu, C. Tang, N. Xu, M. Li, A small molecule transcription factor EB activator ameliorates beta-amyloid precursor protein and Tau pathology in Alzheimer's disease models, Aging Cell 19 (2) (2020) e13069, https://doi.org/10.1111/acel.13069.

[39] D. Wilsker, L. Probst, H.M. Wain, L. Maltais, P.W. Tucker, E. Moran, Nomenclature of the ARID family of DNA-binding proteins, Genomics 86 (2) (2005) 242–251, https://doi.org/10.1016/j.ygeno.2005.03.013.

[40] G. Wang, M. Watanabe, Y. Imai, K. Hara, I. Manabe, K. Maemura, M. Horikoshi, A. Ozeki, C. Itoh, T. Sugiyama, T. Kadowaki, T. Yamazaki, R. Nagai, Associations of variations in the MRF2/ARID5B gene with susceptibility to type 2 diabetes in the Japanese population, J. Hum. Genet. 57 (11) (2012) 727–733, https://doi.org/10.1038/jhg.2012.101.

[41] Y. Okazaki, J. Murray, A. Ehsani, J. Clark, R.H. Whitson, L. Hirose, N. Yanaka, K. Itakura, Increased glucose metabolism in Arid5b(-/-) skeletal muscle is associated with the down-regulation of TBC1 domain family member 1 (TBC1D1), Biol. Res. 53 (1) (2020) 45, https://doi.org/10.1186/s40659-020-00313-3.

[42] P. Wang, Y. Deng, X. Yan, J. Zhu, Y. Yin, Y. Shu, D. Bai, S. Zhang, H. Xu, X. Lu, The role of ARID5B in acute lymphoblastic leukemia and beyond, Front. Genet. 11 (2020) 598, https://doi.org/10.3389/fgene.2020.00598.

[43] E.K. Pickett, C.M. Henstridge, E. Allison, R. Pitstick, A. Pooler, S. Wegmann, G. Carlson, B.T. Hyman, T.L. Spires-Jones, Spread of tau down neural circuits precedes synapse and neuronal loss in the rTgTauEC mouse model of early Alzheimer's disease, Synapse 71 (6) (2017), https://doi.org/10.1002/syn.21965.

[44] J.J. DiGiovanna, K.H. Kraemer, Shining a light on xeroderma pigmentosum, J. Invest. Dermatol. 132 (3 Pt 2) (2012) 785–796, https://doi.org/10.1038/jid.2011.426.

[45] J.E. Cleaver, Defective repair replication of DNA in xeroderma pigmentosum, Nature 218 (5142) (1968) 652–656, https://doi.org/10.1038/218652a0.

[46] Y.S. Krasikova, O.I. Lavrik, N.I. Rechkunova, The XPA protein-life under precise control, Cells 11 (23) (2022), https://doi.org/10.3390/cells11233723.

[47] M. Fousteri, L.H. Mullenders, Transcription-coupled nucleotide excision repair in mammalian cells: molecular mechanisms and biological effects, Cell Res. 18 (1) (2008) 73–84, https://doi.org/10.1038/cr.2008.6.

[48] O.D. Schärer, Nucleotide excision repair in eukaryotes, Cold Spring Harbor Perspect. Biol. 5 (10) (2013) a012609, https://doi.org/10.1101/cshperspect.a012609.

[49] Y. Hou, H. Song, D.L. Croteau, M. Akbari, V.A. Bohr, Genome instability in Alzheimer disease, Mech. Ageing Dev. 161 (Pt A) (2017) 83–94, https://doi.org/10.1016/j.mad.2016.04.005.

[50] H. Wang, S. Lautrup, D. Caponio, J. Zhang, E.F. Fang, DNA damage-induced neurodegeneration in accelerated ageing and alzheimer's disease, Int. J. Mol. Sci. 22 (13) (2021), https://doi.org/10.3390/ijms22136748.

[51] L. Weissman, D.G. Jo, M.M. Sørensen, N.C. de Souza-Pinto, W.R. Markesbery, M.P. Mattson, V.A. Bohr, Defective DNA base excision repair in brain from individuals with Alzheimer's disease and amnestic mild cognitive impairment, Nucleic Acids Res. 35 (16) (2007) 5545–5555, https://doi.org/10.1093/nar/gkm605.

[52] A. Forestier, T. Douki, V. De Rosa, D. Béal, W. Rachidi, Combination of Aβ secretion and oxidative stress in an alzheimer-like cell line leads to the over-expression of the nucleotide excision repair proteins DDB2 and XPC, Int. J. Mol. Sci. 16 (8) (2015) 17422–17444, https://doi.org/10.3390/ijms160817422.

[53] U. Rass, I. Ahel, S.C. West, Defective DNA repair and neurodegenerative disease, Cell 130 (6) (2007) 991–1004, https://doi.org/10.1016/j.cell.2007.08.043.

[54] F. Yang, R. Chen, Sestrin1 exerts a cytoprotective role against oxygen-glucose deprivation/reoxygenation-induced neuronal injury by potentiating Nrf2 activation via the modulation of Keap1, Brain Res. 1750 (2021) 147165, https://doi.org/10.1016/j.brainres.2020.147165.

[55] F. Sanchis-Gomar, Sestrins: novel antioxidant and AMPK-modulating functions regulated by exercise? J. Cell. Physiol. 228 (8) (2013) 1647–1650, https://doi.org/10.1002/jcp.24338.

[56] P.B. Kopnin, L.S. Agapova, B.P. Kopnin, P.M. Chumakov, Repression of sestrin family genes contributes to oncogenic Ras-induced reactive oxygen species up-regulation and genetic instability, Cancer Res. 67 (10) (2007) 4671–4678, https://doi.org/10.1158/0008-5472.Can-06-2466.

[57] H.W. Querfurth, F.M. LaFerla, Alzheimer's disease, N. Engl. J. Med. 362 (4) (2010) 329–344, https://doi.org/10.1056/NEJMra0909142.

[58] D.J. Rawlings, G. Metzler, M. Wray-Dutra, S.W. Jackson, Altered B cell signalling in autoimmunity, Nat. Rev. Immunol. 17 (7) (2017) 421–436, https://doi.org/10.1038/nri.2017.24.

[59] V. Geylis, M. Steinitz, Immunotherapy of Alzheimer's disease (AD): from murine models to anti-amyloid beta (Abeta) human monoclonal antibodies, Autoimmun. Rev. 5 (1) (2006) 33–39, https://doi.org/10.1016/j.autrev.2005.06.007.

[60] E. Maffioletti, D. Tardito, M. Gennarelli, L. Bocchio-Chiavetto, Micro spies from the brain to the periphery: new clues from studies on microRNAs in neuropsychiatric disorders, Front. Cell. Neurosci. 8 (2014) 75, https://doi.org/10.3389/fncel.2014.00075.

[61] G.Y. Ou, W.W. Lin, W.J. Zhao, Construction of long noncoding RNA-associated ceRNA networks reveals potential biomarkers in alzheimer's disease, J Alzheimers Dis 82 (1) (2021) 169–183, https://doi.org/10.3233/jad-210068.

[62] L. Lu, W.Z. Dai, X.C. Zhu, T. Ma, Analysis of serum miRNAs in alzheimer's disease, Am J Alzheimers Dis Other Demen 36 (2021) 15333175211021712, https://doi.org/10.1177/15333175211021712.

[63] E.K. Kim, E.J. Choi, Compromised MAPK signaling in human diseases: an update, Arch. Toxicol. 89 (6) (2015) 867–882, https://doi.org/10.1007/s00204-015-1472-2.

[64] Z. Zhai, F. Wu, F. Dong, A.Y. Chuang, J.S. Messer, D.L. Boone, J.H. Kwon, Human autophagy gene ATG16L1 is post-transcriptionally regulated by MIR142-3p, Autophagy 10 (3) (2014) 468–479, https://doi.org/10.4161/auto.27553.

[65] Z. Zhang, X. Yang, Y.Q. Song, J. Tu, Autophagy in Alzheimer's disease pathogenesis: therapeutic potential and future perspectives, Ageing Res. Rev. 72 (2021) 101464, https://doi.org/10.1016/j.arr.2021.101464.

[66] D.A. Costello, D.M. O'Leary, C.E. Herron, Agonists of peroxisome proliferator-activated receptor-gamma attenuate the Abeta-mediated impairment of LTP in the hippocampus in vitro, Neuropharmacology 49 (3) (2005) 359–366, https://doi.org/10.1016/j.neuropharm.2005.03.009.

[67] D.H. Cho, E.J. Lee, K.J. Kwon, C.Y. Shin, K.H. Song, J.H. Park, I. Jo, S.H. Han, Troglitazone, a thiazolidinedione, decreases tau phosphorylation through the inhibition of cyclin-dependent kinase 5 activity in SH-SY5Y neuroblastoma cells and primary neurons, J. Neurochem. 126 (5) (2013) 685–695, https://doi.org/10.1111/jnc.12264.

[68] D. Tripathy, P. Grammas, Acetaminophen inhibits neuronal inflammation and protects neurons from oxidative stress, J. Neuroinflammation 6 (2009) 10, https://doi.org/10.1186/1742-2094-6-10.

[69] M. Bisaglia, V. Venezia, P. Piccioli, S. Stanzione, C. Porcile, C. Russo, F. Mancini, C. Milanese, G. Schettini, Acetaminophen protects hippocampal neurons and PC12 cultures from amyloid beta-peptides induced oxidative stress and reduces NF-kappaB activation, Neurochem. Int. 41 (1) (2002) 43–54, https://doi.org/10.1016/s0197-0186(01)00136-x.

[70] X.Z. Zhang, X.J. Li, H.Y. Zhang, Valproic acid as a promising agent to combat Alzheimer's disease, Brain Res. Bull. 81 (1) (2010) 3–6, https://doi.org/10.1016/j.brainresbull.2009.09.003.

[71] A.G. Xuan, X.B. Pan, P. Wei, W.D. Ji, W.J. Zhang, J.H. Liu, L.P. Hong, W.L. Chen, D.H. Long, Valproic acid alleviates memory deficits and attenuates amyloid-β deposition in transgenic mouse model of Alzheimer's disease, Mol. Neurobiol. 51 (1) (2015) 300–312, https://doi.org/10.1007/s12035-014-8751-4.

[72] C.S. K, V. Kakoty, K.V. Krishna, S.K. Dubey, D. Chitkara, R. Taliyan, Neuroprotective efficacy of Co-encapsulated rosiglitazone and Vorinostat nanoparticle on streptozotocin induced mice model of alzheimer disease, ACS Chem. Neurosci. 12 (9) (2021) 1528–1541, https://doi.org/10.1021/acschemneuro.1c00022.